NATIONAL ADVISORY COMMITTEE FOR AERONAUTICS

TECHNICAL NOTE 3771

LOW-SPEED WAKE CHARACTERISTICS OF TWO-DIMENSIONAL CASCADE AND ISOLATED AIRFOIL SECTIONS

By Seymour Lieblein and William H. Roudebush

Lewis Flight Propulsion Laboratory
Cleveland, Ohio

Washington

October 1956

NATIONAL ADVISORY COMMITTEE FOR AERONAUTICS

TECHNICAL NOTE 3771

LOW-SPEED WAKE CHARACTERISTICS OF TWO-DIMENSIONAL CASCADE AND ISOLATED AIRFOIL SECTIONS

By Seymour Lieblein and William H. Roudebush

SUMMARY

An analysis of the low-speed wake characteristics of two-dimensional cascade and isolated airfoil sections is presented, based on available experimental data and supplementary theory. Empirical and theoretical variations with downstream distance of such wake properties as minimum velocity, form factor, momentum thickness, full thickness, and total-pressure loss are presented. Information is also included to corroborate theoretical total-pressure-loss relations presented previously, to convert area-averaged losses to mass-averaged losses, and to indicate downstream variations in air outlet angle.

The analysis indicates a general similarity between turbulent cascade and isolated airfoil wake characteristics (except in the variation of momentum thickness). The principal result of the analysis is the observation that the reenergizing of the wake downstream of the blade is very rapid. The major part of the mixing loss and the changes in wake characteristics occur within $\frac{1}{4}$ to $\frac{1}{2}$ chord length behind the blade trailing edge.

INTRODUCTION

An important aspect of current compressor research is the determination and prediction of losses across axial-flow blade rows. As an initial step in this pursuit, attention has been centered on the study of the basic profile loss of blade sections in low-speed two-dimensional flow. It has been shown theoretically (refs. 1 to 4) that, under certain hypotheses, the loss in total pressure across a cascade of blade profiles can be related to the characteristics of the wake formed by the blade-surface boundary layers. In particular (ref. 1), it was shown that the principal wake characteristics involved in the determination of the loss in total pressure are the momentum thickness and the form factor. It was

further shown that these two parameters are significant for the correlation of cascade loss data. A fundamental knowledge of blade-wake characteristics was therefore found to be desirable for detailed analysis of profile losses. A study of blade wakes is also desirable because it can add to the general knowledge of viscous flow across cascade sections and may be useful in understanding and analyzing blade-row interaction effects.

The present report is concerned with the general nature of the wake downstream of low-speed two-dimensional cascade sections. In particular, the variation of certain properties with distance downstream of the trailing edge is studied. Empirical or theoretical variations are determined for such factors as wake minimum velocity, form factor, momentum thickness, full thickness, total-pressure loss, and ratio of mass-averaged to area-averaged loss. The analysis is based on available experimental data and on available or derived theory for both isolated and cascade airfoil sections.

SYMBOLS

a,b,d	constants in equation for minimum velocity
C_L	lift coefficient
c	chord length, ft
f,g	factors in equations for analytical velocity profiles (table III)
H	wake form factor, δ^*/θ
h	constant in relation for wake full thickness
i	incidence angle, angle between inlet-air direction and tangent to blade mean camber line at leading edge, deg
K	wake pseudoenergy factor, k/θ
k	wake pseudoenergy thickness, ft
m	exponent in power velocity profile relation (table III)
n	coordinate normal to outlet-flow direction, ft
P	total pressure, lb/sq ft
$\Delta\bar{P}$	averaged defect in total pressure, lb/sq ft

4000

CI-1 back

p	static pressure, lb/sq ft
s	blade spacing normal to axial direction, ft
s_n	blade spacing normal to outlet-flow direction, ft
U	undisturbed velocity of isolated airfoil
V	air velocity, ft/sec
x	coordinate along outlet-flow direction, ft
Y	ratio $\frac{y}{\left(\frac{\delta_y}{2}\right)}$
y	coordinate normal to axial direction, ft
z	coordinate in axial direction, ft
α	angle of attack, angle between inlet-air direction and blade chord, deg
β	air angle, angle between air velocity and axial direction, deg
δ	wake full thickness, ft
δ^*	wake displacement thickness, ft
θ	wake momentum thickness, ft
$\hat{\theta}$	wake momentum-thickness parameter, $\left(\frac{\theta}{c}\right) \frac{\sigma}{\cos \beta}$
ρ	mass density, lb-sec^2/ft^4
σ	solidity, c/s
$\bar{\omega}_x$	total-pressure-loss coefficient based on outlet free-stream velocity, $\frac{(\Delta \bar{P})_x}{\frac{1}{2} \rho V_{0,x}^2}$
$\bar{\omega}_{1,x}$	total-pressure-loss coefficient based on inlet velocity, $\frac{(\Delta \bar{P})_x}{\frac{1}{2} \rho V_1^2}$

Subscripts:

A	area averaged
l	lower surface
M	mass averaged
min	minimum
n	normal to outlet-flow direction
te	plane of trailing edge
u	upper surface
x	arbitrary outlet location downstream of trailing edge
y	normal to axial direction
z	along axial direction
0	free stream
1	inlet
2	outlet measuring station
∞	far downstream where complete mixing has taken place

DATA CALCULATIONS

The experimental data used for the correlation of wake characteristics of two-dimensional airfoil sections were selected from three sources: (1) two-dimensional cascade tests, (2) isolated airfoil investigations, and (3) mean-radius region of annular cascades with constant annular area across the blade row and free-vortex blading. Such annular cascades were considered acceptable for profile correlations, since essentially equal inlet and outlet axial velocities (as in the two-dimensional case) are obtained at low speed. Possible end-flow or radial-flow effects are minimized by restricting the data to the mean-radius region. Furthermore, only annular data for which no strong circumferential variations of total pressure existed at the blade-row outlet were used. Information concerning the various airfoil sections considered and the various tunnels used is given in tables I and II.

Complete wake data at varying distances downstream of the blade were not available for cascade sections; resulting correlations for the cascade sections were obtained from a succession of discrete data points

from various sources. (Although measurements were obtained at several downstream stations for cascade section 7, it was necessary to treat these data as discrete points because of small variations in incidence angle and an uncertainty in the determination of the limits of the wake.)

Wherever possible, wake characteristics were computed from the experimental wake-velocity distributions obtained from measurements of total and static pressures. In the cascade tests, traverses of total pressure were made either along planes normal to the axial direction or normal to the outlet-flow direction (fig. 1). In both cases, static pressure and flow angle are considered to be constant across the cascade blade spacing. For isolated airfoils, however, variations in static pressure occur normal to the outlet flow. "Free-stream" velocities at the edge of the wake of isolated airfoils (as determined by the decrease in total pressure) are consequently different from the undisturbed velocity. Two-dimensional incompressible flow is assumed throughout in the data calculations and in the analysis.

An illustration of a typical wake velocity profile and definitions of the various wake properties used in the analysis are shown as functions of distance normal to the axial direction in figure 2. The specific assumptions involved in the outlet-flow model of figure 2 are given in appendix A. Corresponding wake properties in a plane normal to the outlet-flow direction for cascades are obtained by replacing y by n, s by s_n, and by deleting the subscript y for all wake quantities in figure 2. All wake properties presented in this report are values in planes normal to the outlet-flow direction. Values computed normal to the axial are corrected to planes normal to the outlet flow by means of the cosine of the angle between the outlet direction and the cascade axis (e.g., $\theta = \theta_y \cos \beta$).

ANALYSIS

The wake of a blade section is formed from the boundary layers on the upper and lower surfaces of the blade, as shown in figure 1. Downstream of the trailing edge, the wake is eventually reenergized through mixing between the wake and the free-stream flow. Inasmuch as a loss in total pressure is involved in the mixing process, the ultimate total pressure at a station far downstream where conditions have become uniform will be less than at the blade trailing edge. The difference in total pressure far downstream and at the blade trailing edge is referred to as the mixing loss.

As the wake is reenergized downstream of the blade, the velocity profile in the wake changes. In particular, the minimum velocity in the trough of the wake and the width of the wake increase with distance

downstream of the blade trailing edge until uniform conditions are finally obtained. Concurrently, changes in the other properties of the wake such as form factor and momentum thickness take place as downstream distance is varied. Although the rate at which a blade wake is reenergized is recognized to depend to some extent upon such additional factors as the initial state of the wake, the free-stream turbulence level, the Reynolds number, and the flow Mach number, these factors are not considered in the present analysis.

Wake Minimum Velocity

A measure of the intensity of the velocity defect in the wake is given by the downstream variation of the wake minimum velocity. Theoretical studies of geometrically similar laminar-wake profiles behind solid bodies (as discussed in ref. 5) have shown that, at some distance downstream of the body, the ratio V_{min}/V_0 (ratio of wake minimum velocity to free-stream velocity) will vary according to the following two relations:

$$\frac{V_{min}}{V_0} = 1 - a\left(\frac{x}{c} + b\right)^{-1/2} - d\left(\frac{x}{c} + b\right)^{-1} \tag{1}$$

or

$$\frac{V_{min}}{V_0} = 1 - a\left(\frac{x}{c} + b\right)^{-1/2} \tag{2}$$

where a, b, and d are constants, c is the characteristic length of the body, and x is the distance downstream of the trailing edge of the body. In reference 5 the variation of V_{min}/V_0 in the laminar wake of the flat plate (of length c) is computed as shown by the dashed line in figure 3.

Analysis of turbulent wake flow (refs. 6 and 7) has also indicated that the minimum velocity ratio in the wake of solid bodies can be approximated in the form of equation (2). Reference 6 shows that the experimental recovery of the wake minimum velocity of several isolated airfoils can be described by equation (2) with $a = 0.1265$ and $b = 0.025$. The variation of minimum velocity ratio obtained is shown by the solid curve in figure 3. As expected, higher values of recovery are obtained for the turbulent wake. The rate of recovery of the minimum velocity in the wake, however, is seen to be at a maximum immediately behind the airfoil trailing edge in both cases.

A plot of the variation of experimental wake minimum velocity ratio with chord-length distance downstream of the trailing edge is shown in figure 4 for available isolated and cascade airfoil data. The cascade airfoil data are indicated by the solid symbols. Only smooth-surface data were used from the various isolated-airfoil references, and free-stream velocities are those at the edge of the wake (generally less than U). The data presented in figure 4 cover a range of blade-chord Reynolds numbers from about 1×10^5 to 5×10^6 (see table I), and therefore represent turbulent wakes. The turbulent-wake data of figure 4 confirm for both cascade and isolated airfoils the previously indicated rapid mixing of the wake immediately downstream of the trailing edge (fig. 3). Approximately 80 percent of the velocity at the edge of the boundary layer is recovered within about 0.2 to 0.5 chord length behind the trailing edge for both the isolated and the cascade airfoils.

4000

Two limiting curves in the form of equation (2) for the isolated airfoils are shown by the dashed curves in figure 4. Constants for the upper curve are given by $a = 0.075$, $b = 0.020$, and for the lower curve by $a = 0.130$ and $b = 0.025$. The lower limiting curve for the isolated airfoil in figure 4 may also serve as a reasonable average curve for the limited cascade data. Although two data points (blade 7 at $x/c = 0.1$ and blade 3 at $x/c = 0.46$) appear noticeably higher than this curve, the indicated departure from the curve is not considered significant. In both cases, the magnitude of the minimum velocity in the wake is not conclusively established, and it is conceivable that the true values of V_{min} may be somewhat less than indicated by the limited profile data. A representative variation of minimum velocity for the cascade airfoil is therefore considered to be

$$\frac{V_{min}}{V_0} = 1 - 0.13\left(\frac{x}{c} + 0.025\right)^{-1/2} \tag{3}$$

The validity of equation (3) for determining the minimum velocity ratio of a cascade section at $x/c = 0$ is somewhat uncertain because of the complex nature of the wake flow in the region of the trailing edge. For cascade sections with conventional trailing-edge thickness (1 to 3 percent of the chord length), strong components of flow normal to the main flow will most likely exist immediately behind the trailing edge. In such cases, measurements in the plane of the trailing edge with conventional-size pitot-type instruments will reveal some average minimum velocity which will not generally be zero. For the isolated airfoils, chord lengths are large (20 to 60 in.) and trailing-edge thicknesses are practically zero, so that smooth flow and well-defined zero minimum velocities are obtained experimentally at the trailing edge.

Wake Form Factor

Information concerning the variation of the wake form factor with distance downstream of the trailing edge has been obtained for the isolated airfoil and the flat plate in references 6 and 8, respectively. Reference 6 shows that the variation of turbulent form factor with distance downstream for isolated airfoils can be related to the variation of the minimum-velocity ratio as given by figure 3. It is shown in that reference that the form factor H can be expressed according to the following relation:

$$1 - \frac{1}{H} = \left(1 - \frac{1}{H_{te}}\right)\left(\frac{\frac{x}{c} + b}{b}\right)^{-1/2} \tag{4}$$

where H_{te} is the value of the form factor at the blade trailing edge and b is the empirical constant obtained for the minimum-velocity variation in equation (2).

In reference 7, the theoretical downstream variation of H for the laminar wake of the flat plate was determined from the results of reference 5. Variations of H with x/c for the laminar wake from reference 7 and for the turbulent wake from reference 6 (from eq. (4) with b = 0.025) are shown in figure 5. Wake form factor is seen to decrease rapidly immediately behind the trailing edge and to approach asymptotically a value of 1 far downstream of the blade.

Experimental values of wake form factor are shown in figure 6 as functions of chord-length distance downstream of the trailing edge for available isolated and cascade airfoils. Also shown in the figure are values of H determined from the theoretical relation of equation (4) for the limiting values of constant b determined from the experimental correlation of figure 4. The upper limiting curve in figure 6 represented by a form factor at the trailing edge H_{te} of 2.8 and b = 0.025 is shown by the upper dashed line, and the lower dashed line represents a lower limiting value with H_{te} = 1.4 and b = 0.020. The available experimental data fall within these two limiting curves. The general relation for H given by equation (4) is thus indicated to be representative of the actual variation of form factor for the turbulent wakes of both isolated and cascade airfoils.

An empirical variation of form factor with downstream distance can thus be established from figure 6 for cascade sections on the basis of equation (3) using a value for b of 0.025 to give

$$1 - \frac{1}{H} = \left(1 - \frac{1}{H_{te}}\right)\left(\frac{\frac{x}{c} + 0.025}{0.025}\right)^{-1/2} \tag{5}$$

Calculated values of the representative variation of form factor according to equation (5) are shown by the solid curves in figure 5 for a range of values of form factor H_{te} at the trailing edge. For values of chord-length distance greater than about 0.4, regardless of the initial value of H_{te}, the local values of form factor are less than 1.2. Specifically, the form-factor equation was originally derived for each leg of the wake. However, the data presented here, as well as in the analysis of reference 6, indicate that the results will be applicable for the entire wake.

In reference 1 it was indicated that the wake-momentum-thickness ratio θ/c can be computed from reported values of experimental total-pressure-loss coefficient, if the wake form factor is known or assumed. The representative curves of figure 5 can be used in the form-factor assumption. At a given measuring station sufficiently far downstream of a cascade (e.g., x/c greater than 0.5), the results of figure 5 indicate that the variation of H with initial value of H_{te} at the trailing edge, and therefore with angle of attack, is not large. This result suggests that, for simplicity, a constant value of H may be considered in the calculation of θ/c from the measured total-pressure loss over the complete range of angle of attack.

Wake Momentum Thickness

The experimental variation of wake-momentum-thickness ratio θ/c with chord-length distance downstream of the trailing edge is shown in figure 7 for the available isolated and cascade airfoil data. For the isolated airfoil, a general decrease in θ/c is observed with downstream distance. However, for the one cascade data curve, a slightly increasing trend is indicated. It was considered desirable, therefore, to investigate the possibility that a basic difference in the general θ/c against x/c characteristics of isolated and cascade airfoils may exist.

The equation for the variation of the momentum thickness of the wake θ is obtained from the conventional boundary-layer momentum equation with zero shear stress as

$$\frac{d\theta}{dx} = - (H + 2) \frac{\theta}{V_0} \frac{dV_0}{dx} \tag{6}$$

where V_0 is the velocity at the outer edge of the wake. From equation (6), it is seen that θ will increase if V_0 decreases and will decrease if V_0 increases. In the flow across isolated airfoils, the wake-outer-edge velocity at the airfoil trailing edge is generally lower

than the undisturbed velocity. The wake-edge velocity then increases with downstream distance until it asymptotically approaches the undisturbed velocity at a theoretically infinite distance downstream (refs. 8 to 10). Typical variations of wake-edge velocity for isolated airfoils are shown in figure 8. The decreasing variation of θ/c with x/c for the isolated airfoil is, therefore, understandable on the basis of equation (6).

For the two-dimensional cascade, if the free-stream velocity is essentially constant in the y-direction between the wakes at all downstream positions (as is generally borne out by experiments), it can be shown from continuity considerations that the free-stream velocity at the edge of the wake will tend to decrease with increasing distance rather than increase as in the case of the isolated airfoils. For example, consider the simple case of an unstaggered cascade of airfoils ($\beta_1 = 0$) at spacing s. The continuity equation between the plane of the blade trailing edge (subscript te) and far downstream where the wake has mixed and the flow is completely uniform across the entire blade spacing (subscript ∞) is given for two-dimensional incompressible flow by (fig. 1)

$$\int_{-s/2}^{s/2} V_{te}\,dy \equiv V_{0,te}\int_{-s/2}^{s/2} \frac{V_{te}}{V_{0,te}}\,dy \equiv V_{0,te}\left[s - \int_{-s/2}^{s/2}\left(1 - \frac{V_{te}}{V_{0,te}}\right)dy\right] = sV_\infty$$

For the assumption of uniform free-stream velocity between the wakes, the integral in the equation is equal to the displacement thickness of the wake δ^*_{te} (fig. 3). Thus, the ratio of free-stream velocity at the trailing edge to free-stream velocity far downstream becomes a simple function of the ratio of wake displacement thickness at the trailing edge to blade spacing

$$\frac{V_{0,te}}{V_\infty} = \frac{1}{1 - (\delta^*_{te}/s)} \tag{7}$$

Values of $V_{0,te}/V_\infty$ as functions of displacement-thickness ratio are shown in figure 9. Therefore the cascade free-stream velocity must decrease with downstream distance for these assumed flow conditions. A corresponding increase in θ/c with x/c should then be obtained for the cascade according to equation (6).

Actually, the variation of θ/c with x/c resulting from the cascade continuity effect can be determined quantitatively from the theoretical flow model of figures 1 and 2. In appendix A, theoretical relations are derived (from the continuity equation and the equations of

4000

momentum in the axial and tangential directions) for finding the local momentum-thickness ratio θ/c as a function of the local form factor H for fixed conditions of σ, $(\theta/c)_{te}$, H_{te}, and β_{te}. Then, from the analytical variation of H with x/c given by equation (5), a corresponding relation for θ/c as a function of x/c is obtained. Calculated variations of θ/c are shown in figure 10 for a range of values of σ, H_{te}, $(\theta/c)_{te}$, and β_{te}. For unstalled cascade flow ($(\theta/c)_{te} < 0.02$; $H_{te} \leq 2.0$, approx.), the increase in wake momentum thickness due to the simplified cascade continuity effect is indicated to be small. Most of the increase occurs immediately behind the trailing edge where the change in form factor, and, therefore, in displacement thickness, is the greatest. For $x/c > 0.2$ very little further change in θ/c occurs for any set of trailing-edge conditions.

Although uniform flow is generally observed downstream of the cascade, it is recognized that flow gradients in the y-direction may occur in the immediate region of the trailing edge. Such gradients may alter the influence of the continuity effect on the wake-edge velocity variation and make the prediction of the θ/c variation uncertain in the region of the trailing edge. In general, for a given airfoil section, the variation of θ/c will be a result of the combined effects of the continuity condition and the normal static-pressure variations. According to consideration of the downstream variation of mixing loss, as indicated in a later section, however, it is likely that some increase in θ/c does occur immediately downstream of the trailing edge in a real two-dimensional flow. Additional experimental analysis is necessary to conclusively establish the variation of θ/c for the cascade.

Wake Full Thickness

The full width of the wake is generally considered to be the extent of the region where the total pressure shows a defect. For practical purposes in the analysis, the wake limits were arbitrarily based on the points where the velocity in the wake was equal to 0.995 of the free-stream velocity for the sections for which profile data were available. The downstream variation of experimental wake-full-thickness ratio δ/c obtained for the available data (only isolated airfoil data were available) is shown in figure 11(a). According to these data, the approximate relation $\delta/c \propto (x/c + h)^{1/2}$ obtained from turbulent-wake theory (refs. 7 and 9) does not appear to be valid for $x/c < 1$.

The plot of the increase in δ/c downstream of the trailing edge shown in figure 11(b) indicates that a single curve may be obtained to approximate the downstream increase in full thickness. A simple empirical relation for δ/c up to $x/c = 2$ can then be given as

$$\left(\frac{\delta}{c}\right)_x = \left(\frac{\delta}{c}\right)_{te} + 0.052\left(\frac{x}{c}\right)^{0.75} \quad (8)$$

The empirical variation for increase in δ/c is shown by the dashed line in figure 11(b).

Although the absence of experimental data prevents any conclusions concerning the full-thickness variation of the wakes of cascade sections, it is believed that the empirical increase in δ/c derived from the isolated-airfoil data (fig. 11(b)) may also be representative of the cascade airfoil for equivalent values of trailing-edge full thickness. This belief is based on the observation (established from the plots of wake minimum velocity and form factor in figs. 4 and 6) that the mixing processes in the wakes of conventional cascade and isolated airfoils are similar. However, experimental evidence is necessary to establish the trend for the cascade airfoil.

4000

Air Outlet Angle

Another important property of the cascade flow that is affected by the downstream variation of the wake characteristics is the air outlet angle. For the assumed flow model (fig. 2 and appendix A), conservation of momentum in the y-direction requires that the air outlet angle β_x increase with distance downstream of the trailing edge according to equation (A19) in appendix A. Calculated variations of β_x with x/c are shown in figure 12 for several values of β_{te}, $\hat{\theta}_{te}$, and H_{te}. According to these theoretical results, essentially no downstream changes in air outlet angle should occur due to the cascade continuity effect for locations beyond about $\frac{1}{4}$ chord length behind the trailing edge.

Total-Pressure Loss

According to the theoretical developments of reference 1, the total-pressure-loss coefficient in a plane at an arbitrary distance x downstream of the trailing edge can be expressed as

$$\bar{\omega}_{1,x} \equiv \frac{(\Delta\bar{P})_x}{\frac{1}{2}\rho V_1^2} = \left(\frac{\cos\beta_1}{\cos\beta_{te}}\right)^2\left(\frac{\cos\beta_{te}}{\cos\beta_x}\right)^2 2\hat{\theta}_x\left(\frac{2H_x}{3H_x - 1}\right)(1 - \hat{\theta}_x H_x)^{-3} \quad (9)$$

where $\hat{\theta}_x = (\theta/c)_x\,\sigma/\cos\beta_x$ and $(\Delta\bar{P})_x$ is the mass-averaged loss in total pressure up to the arbitrary station (eq. (13)). In equation (9) it is seen that if the variations of H_x, $\hat{\theta}_x$, and β_x can be determined

as functions of distance x/c, then the corresponding loss coefficient can be computed as a function of x/c. An empirical variation of H_x with x/c has been established previously in equation (5). Theoretical equations for the variation of $\hat{\theta}_x$ and β_x are developed in appendix A. Calculated variations of $\hat{\theta}_x$ against x/c, as shown in figure 13, were generally similar to the theoretical variations of $(\theta/c)_x$ shown in figure 10.

4000

Calculated values of the downstream variation of loss coefficient expressed in the form $\bar{\omega}_{1,x}(\cos \beta_{te}/\cos \beta_1)^2$, as obtained from equation (9), are shown in figure 14 for a range of values of $\hat{\theta}_{te}$, H_{te}, and β_{te}. These results show, as suspected previously, that a rapid rise in total-pressure loss occurs immediately behind the trailing edge. According to these calculations, approximately 90 percent of the mixing loss has occurred at $\frac{1}{2}$ chord-length distance downstream of the blade.

The primary factor governing the magnitude of the relative increase in loss is found to be the wake form factor at the trailing edge. This observation is demonstrated in figure 15, which shows the variation with x/c of the ratio of the loss at station x given by $(\Delta\bar{P})_x$ to the loss at the trailing edge $(\Delta\bar{P})_{te}$ obtained from equation (9) as

$$\frac{(\Delta\bar{P})_x}{(\Delta\bar{P})_{te}} = \frac{\bar{\omega}_{1,x}}{\bar{\omega}_{1,te}} = \frac{\hat{\theta}_x}{\hat{\theta}_{te}}\left(\frac{\cos \beta_{te}}{\cos \beta_x}\right)^2\left(\frac{3 - \frac{1}{H_{te}}}{3 - \frac{1}{H_x}}\right)\left(\frac{1 - \hat{\theta}_{te}H_{te}}{1 - \hat{\theta}_x H_x}\right)^3 \qquad (10)$$

In equation (10), $\hat{\theta}_x$ and β_x were obtained from the theoretical developments of appendix A, and H_x was obtained from equation (5).

Furthermore, it is noted that the use of definitions of loss coefficient other than $\bar{\omega}_{1,x}$ may not necessarily indicate true downstream variations of the loss in total pressure. For example, a loss coefficient based on outlet velocity $\bar{\omega}_x = (\Delta\bar{P})_x \Big/ \frac{1}{2}\rho V_{0,x}^2$ is frequently used in cascade practice. For this definition, the ratio of loss coefficients $\bar{\omega}_x/\bar{\omega}_{te}$ is given by

$$\frac{\bar{\omega}_x}{\bar{\omega}_{te}} = \frac{(\Delta\bar{P})_x}{(\Delta\bar{P})_{te}}\left(\frac{V_{0,te}}{V_{0,x}}\right)^2 \qquad (11)$$

Since $(V_{0,te}/V_{0,x})$ will vary with x/c (the relation between $V_{0,x}$ and $V_{0,te}$ as a function of wake characteristics is obtained from eqs. (A12) and (A15) in appendix A), a true ratio of total pressures will not be obtained with downstream distance.

The variation of total-pressure loss given by equation (9) can also shed some light on the question of the probable downstream variation of the cascade wake-momentum-thickness ratio, θ/c. As indicated previously (fig. 10), theoretical calculations based on the assumed flow model for the cascade revealed an increase in θ/c immediately behind the blade, but the limited experimental data (fig. 7) were not sufficient to establish any trends in this region. It is possible nevertheless to interpret the experimental data of figure 7 as suggesting a constant value of θ/c with x/c. If constant values of θ/c (in conjunction with the empirical variation of H_x (eq. (5)) and the theoretical variation of β_x are used in equation (10), however, unrealistic values of loss ratio are obtained. It seems likely, therefore, that some increase in θ/c does occur immediately downstream of the trailing edge in the actual two-dimensional cascade flow.

Mass-Averaged and Area-Averaged Total-Pressure Defect

In experimental cascade practice, the loss in total pressure in the wake at the measuring station is often expressed in terms of an area average, where

$$\Delta\bar{P}_A = \frac{1}{s}\int_{-s/2}^{s/2} (P_0 - P)dy \tag{12}$$

In theoretical analyses of cascade losses (ref. 1, e.g.), the loss in total pressure is expressed in terms of a mass-averaged defect given by

$$\Delta\bar{P}_M = \frac{\int_{-s/2}^{s/2} \rho V_z (P_0 - P)dy}{\int_{-s/2}^{s/2} \rho V_z dy} \tag{13}$$

It is convenient, therefore, to determine the variation of the relation between mass and area averages of total-pressure defect with downstream distance so that the available experimental data and theoretical relations can be readily compared.

An insight into the comparison of the two averaging methods was obtained by investigating the ratio of mass-averaged to area-averaged total-pressure defect of several representative analytical wake velocity profiles shown in figures 16(a) to (d). Equations for the velocity distribution V/V_0 in each wake profile are given in table III. (The wake profiles are symmetrical about the point of minimum velocity at $Y = y/\left(\frac{\delta_y}{2}\right) = 0.$) The general equation for the ratio of mass-averaged to area-averaged defect $(\Delta\bar{P})_M/(\Delta\bar{P})_A$, henceforth called the averaging ratio, is developed in appendix B, and the specific equations obtained for each velocity profile are listed in table III.

The theoretical averaging ratio, as indicated in table III, depends on the magnitude of the minimum velocity ratio V_{min}/V_0 and the ratio δ_y/s_n of the wake full thickness δ_y to any arbitrary spacing interval s_n normal to the outlet flow. Calculated variations of the averaging ratio against wake-minimum-velocity ratio are shown for the analytical profiles in figure 17(a) for two values of the full-thickness to spacing ratio δ/s_n. It is seen that finite values of averaging ratio are obtained in the limit as $\delta \to 0$ or $s_n \to \infty (\delta/s_n = 0)$.

The effect of the wake full-thickness to spacing ratio on the averaging ratio is shown in figure 17(b), which shows a plot of the variation of the averaging ratio as an arithmetic average value of all four profiles against δ/s_n. In figure 17(b), the averaging ratio is expressed as the ratio of the value of the averaging ratio at any δ/s_n to the value of the arbitrarily selected reference averaging ratio at $\delta/s_n = 0$.

Experimental values of averaging ratio are shown in figure 18(a) for the available cascade and isolated airfoils. For the cascade airfoils, the interval over which the loss integrations were conducted was taken equal to the normal spacing between blades (s_n in fig. 1). For the isolated airfoil, the interval of integration was arbitrarily taken between the points where the outlet velocity attained the free-stream value. In keeping with the previous definition of wake full thickness, the width of the wake was established at the points where the wake V/V_0 attained a value of 0.995. Thus, for the isolated airfoils, the ratio δ/s_n was somewhat less than 1. Also shown in the figure by the dashed lines are the calculated variations of averaging ratio determined for representative analytical profiles for limiting values of δ/s_n obtained in the experimental data.

The experimental values of averaging ratio in figure 18(a) were corrected to a common reference value of $\delta/s_n = 0$ by dividing the averaging-ratio values of figure 18(a) by the appropriate ratios of the averaging ratio given in figure 17(b). The corresponding corrected values are shown in figure 18(b). It was possible, therefore, to derive a satisfactory empirical variation of the averaging ratio with minimum-velocity ratio for the reference condition of zero δ/s_n as shown by the solid curve in figure 18(b).

Derived variations of $(\Delta\bar{P})_M/(\Delta\bar{P})_A$ over a complete range of full-thickness to spacing ratios were then obtained from the empirical curve found in figure 18(b) for $\delta/s_n = 0$ in conjunction with the averaging-ratio ratios presented in figure 17(b), as shown in figure 19(a). Furthermore, since minimum-velocity ratio is expressed analytically as a function of the chord-length distance downstream of the blade (from fig. 4), the averaging ratios can then also be expressed as a function of chord-length distance downstream from figure 19(a) and equation (3), as shown in figure 19(b). Thus, from figure 19, if the ratio δ/s_n is known ($\delta/s_n = \delta_y/s$) and either the wake-minimum-velocity ratio or the chord-length distance downstream of the trailing edge is known, the ratio of mass-averaged to area-averaged total-pressure defect can be determined. According to these results, for measuring stations located between $\frac{1}{2}$ and 1 chord length downstream of the blade trailing edge, the ratio of mass-averaged to area-averaged defect in total pressure for conventional cascade sections can vary from about 0.88 to about 0.95.

In most cases, the averaging ratio for the total-pressure defect presented in figure 19 will be identical to the averaging ratio of the total-pressure-loss coefficient. For the loss coefficient based on inlet velocity $\bar{\omega}_{1,x}$ (defined in eq. (9)), since $(\bar{V}_1^2)_M = (\bar{V}_1^2)_A$,

$$\frac{(\bar{\omega}_{1,x})_M}{(\bar{\omega}_{1,x})_A} \equiv \frac{(\Delta\bar{P})_M}{(\Delta\bar{P})_A}$$

On the other hand, for example, if a loss coefficient is defined as $(\Delta\bar{P})_A \Big/ \frac{1}{2}\rho\bar{V}_A^2$ where $\bar{V}_A^2$ is the area-averaged outlet velocity, the conversion to a mass-averaged loss coefficient will also involve the relation between the reference velocities of the area-averaged loss coefficient and the desired mass-averaged coefficient. The appropriate relations between the reference velocities will generally be expressible in terms of the wake characteristics from consideration of the flow model of figure 2.

4000

K-H Relation in Theoretical Loss Equation

In order to obtain a useful theoretical equation for loss coefficient based on the wake characteristics of $\hat{\theta}_x$ and H_x only (as in eq. (9), e.g.), it was convenient in reference 1 to use an approximate relation between a pseudoenergy factor K (fig. 2) and the form factor H determined analytically from the power velocity profile as

$$K = \frac{H+1}{3H-1} \tag{14}$$

Additional experimental data are now presented to investigate further the validity of this approximation.

A comparison of values of K against H obtained from numerical integration of the available experimental wake velocity profiles and from theoretical calculations of the analytical profiles of figures 16(a) to (e) are shown in figure 20. The experimental data were taken at downstream positions for which the wake minimum velocity is greater than zero (x/c greater than 0.02). Equations for V/V_0 and K for these analytical profiles are given in table III.

The final measure of the validity of the K-H relation is obtained from a comparison between the values of loss coefficient obtained from the theoretical equation in conjunction with known experimental values of $\hat{\theta}$ and H, and the values of loss coefficient obtained from direct integration of the total-pressure defect. Loss coefficients computed by the theoretical equation (eq. (42) in ref. 1) checked with those determined by direct integration (eqs. (2) and (40) in ref. 1) within about ±1 percent for the available cascade data considered herein. The K-H relation of reference 1, therefore, constitutes a valid approximation for downstream cascade-measuring-station locations at $x/c > 0.02$.

In the plane of the trailing edge (x/c = 0) where the wake minimum velocity is zero, it was found from the isolated airfoils that the experimental K values were somewhat larger than the values in figure 20. A different H-K relation may therefore exist at the trailing edge when $V_{min}/V_0 = 0$. However, if loss coefficients for complete mixing are desired, the K-H relation is of no consequence since only the wake $\hat{\theta}_{te}$ and H_{te} are required (ref. 1).

SUMMARY OF RESULTS

In the preceding analysis of the low-speed wake characteristics of two-dimensional isolated and cascade airfoils, it is shown that empirical or theoretical relations can be obtained for the variation of various

properties of the wake with distance downstream of the trailing edge. For the range of airfoil geometries and flow conditions covered, a similarity of the wake developments of the isolated airfoil and the cascade airfoil was observed in the downstream variation of the wake minimum velocity and wake form factor. However, an apparent region of dissimilarity in the wake developments was found in the variation of momentum thickness. Both theory and limited experimental data indicate that cascade wake momentum thickness in two-dimensional flow tends to show a slight increase with downstream distance, while, for the isolated airfoil, wake momentum thickness decreases. However, additional experimental data are necessary to conclusively establish the momentum-thickness variation of the cascade airfoil. Data were not available to compare the variations of wake full thickness.

The principal result of the analysis is the observation that most of the reenergizing of the wake occurs within a relatively short distance behind the blade. For example, within $\frac{1}{4}$ chord length downstream of the blade, the experimental minimum velocity in the wake has attained 0.75 to 0.85 of the free-stream value, and the experimental wake form factor has fallen off to 1.2 or less. The greater part of the downstream variations in wake momentum thickness, air outlet angle, and mixing loss are also indicated to occur within a short distance behind the blade. For conventional sections, practically the entire additional loss in total pressure arising from the mixing of the wake is incurred within $\frac{1}{2}$ chord-length distance behind the blade. Theoretical calculations showed that the downstream increase in loss resulting from the wake mixing is primarily a function of the form factor of the wake at the trailing edge.

Experimental loss data were utilized to verify the validity of one of the principal assumptions in the theoretical cascade loss developments of reference 1, which were used as the basis of the theoretical developments in the present report. Theory and experimental data were also used to derive variations of the ratio of mass-averaged to area-averaged total-pressure loss as a function of wake minimum velocity or downstream distance.

CONCLUDING REMARKS

The results of the preceding analysis of wake characteristics can find application in the interpretation and utilization of two-dimensional cascade data in several respects. Since variation of mixing loss with downstream distance can be large, it is desirable for proper comparison of losses from different configurations to take into account any differences in measuring-station location. Measurements of cascade blade losses usually taken between $\frac{1}{2}$ to 1 chord length behind the blade, according to the mixing-loss variations determined in the analysis, will include

practically the entire mixing loss. Furthermore, it may be desired to utilize cascade loss data obtained at a downstream location to correlate blade boundary-layer characteristics with the velocity distribution or velocity diffusion on the blade surfaces. For such correlations, corrections for the differences in wake and loss characteristics between the measuring station and the blade trailing edges should be considered. The deduced ratios of mass-averaged to area-averaged total-pressure loss (fig. 19) can be utilized in cascade investigations to permit the reduction of the loss data in terms of the simplified area-averaged loss coefficient and then to convert these data to mass-averaged loss coefficients as indicated by the derived relations.

Knowledge of blade-wake characteristics may also be helpful in compressor research. Although it is recognized that such compressor factors as compressibility and secondary and unsteady flows will influence the wake development in the compressor, the airfoil-section data presented may be drawn upon to gain an insight into the general behavior of the wake of blade sections. Such information concerning the variation of the wake full thickness and the wake minimum velocity may be useful for preliminary studies of blade-row interference effects (relative unsteady motions and wake interactions). Experimental investigations of wake profiles relative to rotating blade rows can also make use of the fundamental wake characteristics of blade sections. Finally, the results point to the important part that may be played by mixing losses in the development of the total-loss picture in the compressor.

In view of the very limited experimental information available for cascade sections, it is felt that additional data would be desirable to more conclusively define the development of the wake in the cascade. Furthermore, since the correlations obtained herein have all been based on low-speed flow, the effect of compressibility on the wake development should be determined in order to permit a more significant application to the compressor configuration. It is known that such wake characteristics as form factor and mixing loss, for example, will vary significantly with local Mach number (refs. 2 and 18). Information concerning the effects of changing free-stream turbulence level and blade-chord Reynolds number on the wake developments should also be of interest.

Lewis Flight Propulsion Laboratory
National Advisory Committee for Aeronautics
Cleveland, Ohio, June 18, 1956

APPENDIX A

THEORETICAL VARIATION OF WAKE PROPERTIES (θ/c), $\hat{\theta}$, and β

The theoretical downstream variations of such wake properties as the momentum-thickness ratio $(\theta/c)_x$, the momentum-thickness parameter $\hat{\theta}_x$, the total-pressure loss $(\Delta\bar{P})_x$, and also the variation of the outlet flow angle β_x are based on a model of the outlet flow at any arbitrary distance downstream of the cascade (within about $1\frac{1}{2}$ chord lengths) as illustrated in figures 1 and 2. Specifically, the assumptions made in the development of the equations (as in ref. 1) are: (1) the flow is two-dimensional and incompressible, (2) the inlet flow is uniform across the blade spacing (y-direction), (3) the outlet static pressure and flow angle are constant across the entire blade spacing, (4) the outlet total pressure is constant in the free stream outside the wake, and (5) the outlet free-stream total pressure is equal to the inlet total pressure.

4000

Momentum-Thickness Ratio

For the type of flow illustrated by the theoretical flow model of figures 1 and 2, consideration of axial momentum requires that

$$\int_{-s/2}^{s/2} \rho V_{z,x}^2 \, dy + s p_x = \text{constant} \tag{A1}$$

From the Bernoulli equation, since p_x is constant in the direction of y,

$$p_x = P_x - \frac{1}{2}\rho V_x^2 = P_{0,x} - \frac{1}{2}\rho V_{0,x}^2$$

$$= \text{constant} - \frac{1}{2}\rho V_{0,x}^2 \tag{A2}$$

Substituting for p_x in (A1) from (A2)

$$\int_{-s/2}^{s/2} \rho V_{z,x}^2 \, dy - s\,\frac{1}{2}\rho V_{0,x}^2 = \text{constant}$$

or

$$V_{0,x}^2\left[\int_{-s/2}^{s/2}\left(\frac{V_{z,x}}{V_{0,x}}\right)^2 dy - \frac{s}{2}\right] = \text{constant} \tag{A3}$$

But

$$\int_{-s/2}^{s/2}\left(\frac{V_{z,x}}{V_{0,x}}\right)^2 dy = \cos^2\beta_x \int_{-s/2}^{s/2}\left(\frac{V_x}{V_{0,x}}\right)^2 dy$$

$$= \cos^2\beta_x \left\{s - \int_{-s/2}^{s/2}\left[1 - \left(\frac{V_x}{V_{0,x}}\right)^2\right] dy\right\}$$

$$= \cos^2\beta_x \left\{s - \int_{-\delta_{l,y}}^{\delta_{u,y}}\left[1 - \left(\frac{V_x}{V_{0,x}}\right)^2\right] dy\right\}$$

$$= \cos^2\beta_x \left[s - \int_{-\delta_{l,y}}^{\delta_{u,y}}\left(1 - \frac{V_x}{V_{0,x}}\right)\left(\frac{V_x}{V_{0,x}}\right)dy - \int_{-\delta_{l,y}}^{\delta_{u,y}}\left(1 - \frac{V_x}{V_{0,x}}\right) dy\right]$$

$$= \cos^2\beta_x \left(s - \theta_{y,x} - \delta_{y,x}^*\right) \tag{A4}$$

Since

$$\left.\begin{aligned} \theta_x &= \theta_{y,x} \cos \beta_x \\ \text{and} \qquad \delta_x^* &= \delta_{y,x}^* \cos \beta_x \end{aligned}\right\} \tag{A5}$$

equation (A4) becomes, with $\sigma = c/s$,

$$\int_{-s/2}^{s/2}\left(\frac{V_{z,x}}{V_{0,x}}\right)^2 dy = s\cos\beta_x\left[\cos\beta_x - \left(\frac{\theta}{c}\right)_x\sigma - \left(\frac{\delta^*}{c}\right)_x\sigma\right]$$

$$= s\cos\beta_x\left[\cos\beta_x - \sigma\left(\frac{\theta}{c}\right)_x(1 + H_x)\right] \qquad (A6)$$

Substituting (A6) into (A3) gives

$$V_{0,x}^2\left\{\cos\beta_x\left[\cos\beta_x - \sigma\left(\frac{\theta}{c}\right)_x(1 + H_x)\right] - \frac{1}{2}\right\} = \text{constant} \qquad (A7)$$

For the conservation of momentum in the y-direction,

$$\int_{-s/2}^{s/2} V_{z,x}V_{y,x}dy = \text{constant} \qquad (A8)$$

From (A8)

$$\int_{-s/2}^{s/2} V_{z,x}V_{y,x}dy = \tan\beta_x\int_{-s/2}^{s/2} V_{z,x}^2 dy$$

$$= V_{0,x}^2\tan\beta_x\int_{-s/2}^{s/2}\left(\frac{V_{z,x}}{V_{0,x}}\right)^2 dy = \text{constant} \qquad (A9)$$

Then, using (A6) in (A9) gives

$$V_{0,x}^2\sin\beta_x\left[\cos\beta_x - \sigma\left(\frac{\theta}{c}\right)_x(1 + H_x)\right] = \text{constant} \qquad (A10)$$

For the conservation of mass flow,

$$\int_{-s/2}^{s/2} V_{z,x}dy = \text{constant} \qquad (A11)$$

From equation (A11)

$$\int_{-s/2}^{s/2} V_{z,x}\,dy = V_{0,x}\cos\beta_x \int_{-s/2}^{s/2} \frac{V_x}{V_{0,x}}\,dy = V_{0,x}\cos\beta_x\left[s - \int_{-s/2}^{s/2}\left(1 - \frac{V_x}{V_{0,x}}\right)dy\right]$$

$$= V_{0,x}\cos\beta_x\,(s - \delta^*_{y,x}) = V_{0,x}\left[\cos\beta_x - \sigma\left(\frac{\delta^*}{c}\right)_x\right] = \text{constant}$$

4000

or

$$V_{0,x}\left[\cos\beta_x - \sigma\left(\frac{\theta}{c}\right)_x H_x\right] = \text{constant} \qquad \text{(A12)}$$

$V_{0,x}$ can be eliminated from equations (A7) and (A10) by the use of equation (A12) to give

$$\frac{\cos\beta_x\left[\cos\beta_x - \sigma\left(\frac{\theta}{c}\right)_x (1 + H_x)\right] - \frac{1}{2}}{\left[\cos\beta_x - \sigma\left(\frac{\theta}{c}\right)_x H_x\right]^2} = \text{constant} \qquad \text{(A13)}$$

and

$$\frac{\sin\beta_x\left[\cos\beta_x - \sigma\left(\frac{\theta}{c}\right)_x (1 + H_x)\right]}{\left[\cos\beta_x - \sigma\left(\frac{\theta}{c}\right)_x H_x\right]^2} = \text{constant} \qquad \text{(A14)}$$

Equations (A13) and (A14) provide two equations in the three unknowns $(\theta/c)_x$, H_x, and β_x for given values of the constants. The values of the constants can be determined from a known set of values of the variables at any station x. For the calculations, the reference location was taken at the trailing edge. Thus, the constants in equations (A13) and (A14) were determined as the quantities in the left side of the equations at the trailing edge, station te.

Of the three unknowns in equations (A13) and (A14), H_x has already been determined empirically as a function of H_{te} and x/c in equation (5). Therefore, with this prescribed variation of H_x, equations (A13) and (A14) can be solved by a double iteration process for the variation

of $(\theta/c)_x$ with x/c for any set of trailing-edge conditions, β_{te}, H_{te}, and $(\theta/c)_{te}$. Solutions for $(\theta/c)_x$, however, can be obtained more readily, as indicated in the succeeding developments, from consideration of the equations in terms of the momentum-thickness parameter $\hat{\theta}_x$.

Momentum-Thickness Parameter

The momentum-thickness parameter $\hat{\theta}_x$ is defined as

$$\hat{\theta}_x = \left(\frac{\theta}{c}\right)_x \frac{\sigma}{\cos \beta_x} \tag{A15}$$

In terms of $\hat{\theta}_x$, equations (A13) and (A14) become, respectively,

$$\frac{1 - \hat{\theta}_x(1 + H_x) - \dfrac{1}{2\cos^2\beta_x}}{(1 - \hat{\theta}_x H_x)^2} = \text{constant} = K_1 \tag{A16}$$

and

$$\frac{\sin \beta_x \left[1 - \hat{\theta}_x(1 + H_x)\right]}{\cos \beta_x (1 - \hat{\theta}_x H_x)^2} = \text{constant} = \sqrt{K_2} \tag{A17}$$

With the use of the parameter $\hat{\theta}_x$, β_x can be eliminated from equations (A16) and (A17) to give

$$2\left[1 - \hat{\theta}_x(1+H_x)\right]^2\left\{\left[1 - \hat{\theta}_x(1+H_x)\right] - K_1(1-\hat{\theta}_x H_x)^2\right\} = K_2(1-\hat{\theta}_x H_x)^4 + \left[1 - \hat{\theta}_x(1+H_x)\right]^2 \tag{A18}$$

Equation (A18) can be solved for $\hat{\theta}_x$ by a single iteration process for the prescribed variation of H_x (eq. (5)) and a set of trailing-edge conditions, H_{te}, $\hat{\theta}_{te}$, and β_{te}.

Outlet Flow Angle

The variation of outlet flow angle β_x can be readily determined from either equation (A16) or (A17). From equation (A17), for example, it is obtained that

4000

$$\beta_x = \tan^{-1}\left\{\tan \beta_{te}\left(\frac{1 - \hat{\theta}_x H_x}{1 - \hat{\theta}_{te} H_{te}}\right)^2\left[\frac{1 - \hat{\theta}_{te}(1 + H_{te})}{1 - \hat{\theta}_x(1 + H_x)}\right]\right\} \quad \text{(A19)}$$

Values of β_x as a function of x/c are then computed for fixed values of β_{te}, H_{te}, and $\hat{\theta}_{te}$ from the downstream variations of $\hat{\theta}_x$ (from eq. (A18)) and H_x (from eq. (5)).

Furthermore, from the variations of $\hat{\theta}_x$ and β_x determined from equations (A18) and (A19), respectively, families of curves of $(\theta/c)_x$ against x/c can be obtained for fixed values of $\hat{\theta}_{te}$, H_{te}, and β_{te} by varying σ and $(\theta/c)_{te}$ so that $\sigma(\theta/c)_{te} = \hat{\theta}_{te} \cos \beta_{te}$.

APPENDIX B

MASS-AVERAGED AND AREA-AVERAGED TOTAL-PRESSURE DEFECT

The area-averaged defect in total pressure in a plane normal to the axial direction (figs. 1 and 3) is given by

$$\Delta\bar{P}_A = \frac{1}{s}\int_{-s/2}^{s/2} (P_0 - P)dy \tag{B1}$$

or, from consideration of the Bernoulli equation and the pressure variations of figure 2, by

$$\Delta\bar{P}_A = \frac{1}{s}\int_{-\delta_{l,y}}^{\delta_{u,y}} \frac{\rho}{2} (V_0^2 - V^2)dy \tag{B2}$$

For the analytical wake velocity profiles of figure 15, since the profiles are symmetrical about the point of minimum velocity at $y = 0$, equation (B2) can be expressed for the half wake as

$$\Delta\bar{P}_A = \frac{1}{2}\rho V_0^2 \frac{2}{s}\int_0^{\delta_y/2}\left(1 - \frac{V^2}{V_0^2}\right)dy = \frac{1}{2}\rho V_0^2\left(\frac{\delta_y}{s}\right)\int_0^1\left(1 - \frac{V^2}{V_0^2}\right)dY \tag{B3}$$

where

$$Y = y/(\delta_y/2)$$

The mass-averaged defect in total pressure is given by

$$\Delta\bar{P}_M = \frac{\int_{-s/2}^{s/2} \rho V_z(P_0 - P)dy}{\int_{-s/2}^{s/2} \rho V_z dy} \tag{B4}$$

or, for the symmetrical profile, since β is constant along y, by

$$\Delta\bar{P}_M = \frac{\frac{1}{2}\rho V_0^2 \int_0^{\delta_y/2} \frac{V}{V_0}\left(1 - \frac{V^2}{V_0^2}\right) dy}{\int_0^{\delta_y/2} \frac{V}{V_0}\, dy + \frac{1}{2}(s - \delta_y)} = \frac{\frac{1}{2}\rho V_0^2 \left(\frac{\delta_y}{2}\right) \int_0^1 \frac{V}{V_0}\left(1 - \frac{V^2}{V_0^2}\right) dY}{\frac{\delta_y}{2}\int_0^1 \frac{V}{V_0}\, dY + \frac{1}{2}(s - \delta_y)}$$

$$= \frac{\frac{1}{2}\rho V_0^2 \left(\frac{\delta_y}{s}\right) \int_0^1 \left(\frac{V}{V_0} - \frac{V^3}{V_0^3}\right) dY}{\left(1 - \frac{\delta_y}{s}\right) + \frac{\delta_y}{s}\int_0^1 \frac{V}{V_0}\, dY} \tag{B5}$$

The ratio of mass-averaged to area-averaged total-pressure defect is then obtained from equations (B5) and (B3) as, since $\delta_y/s = \delta/s_n$,

$$\frac{\Delta\bar{P}_M}{\Delta\bar{P}_A} = \frac{\int_0^1 \left(\frac{V}{V_0} - \frac{V^3}{V_0^3}\right) dY}{\left[\left(1 - \frac{\delta}{s_n}\right) + \frac{\delta}{s_n}\int_0^1 \frac{V}{V_0}\, dY\right]\left(1 - \int_0^1 \frac{V^2}{V_0^2}\, dY\right)} \tag{B6}$$

Equations for the averaging ratios of the analytical wake velocity profiles of figures 15(a) to (d) as determined from equation (B6) are given in table III.

REFERENCES

1. Lieblein, Seymour, and Roudebush, William H.: Theoretical Loss Relations for Low-Speed Two-Dimensional Cascade Flow. NACA TN 3662, 1956.

2. Stewart, Warner L.: Analysis of Two-Dimensional Compressible-Flow Loss Characteristics Downstream of Turbomachine Blade Rows in Terms of Basic Boundary-Layer Characteristics. NACA TN 3515, 1955.

3. Schlichting, Hermann: Problems and Results of Investigations on Cascade Flow. Jour. Aero. Sci., vol. 21, no. 3, Mar. 1954, pp. 163-178.

4. MacGregor, Charles A.: Two-Dimensional Losses in Turbine Blades. Jour. Aero. Sci., vol. 19, no. 6, June 1952, pp. 404-408.

5. Goldstein, S.: On the Two-Dimensional Steady Flow of a Viscous Fluid Behind a Solid Body, Appendix by A. Fage. Proc. Roy. Soc. (London), ser. A, vol. 142, no. A 847, Nov. 1, 1953, pp. 545-573.

6. Spence, D. A.: Growth of the Turbulent Wake Close Behind an Aerofoil at Incidence. C.P. No. 125, British A.R.C., 1952.

7. Townsend, A. A.: Momentum and Energy Diffusion in the Turbulent Wake of a Cylinder. Proc. Roy. Soc. (London), ser. A, vol. 197, no. A 1048, May 11, 1949, pp. 124-140.

8. Preston, J. H., and Sweeting, N. E.: The Experimental Determination of the Boundary Layer and Wake Characteristics of a Simple Joukowski Aerofoil, with Particular Reference to the Trailing Edge Region. R. & M. No. 1998, British A.R.C., 1943.

9. Silverstein, Abe: Wake Characteristics and Determination of Profile Drag by the Momentum Method. Proc. Fifth Int. Cong. Appl. Mech., 1938, pp. 403-409.

10. Squire, H. B., and Young, A. D.: The Calculation of the Profile Drag of Aerofoils. R. & M. No. 1838, British A.R.C., Nov. 1937.

11. Briggs, William B.: Effect of Mach Number on the Flow and Application of Compressibility Corrections in a Two-Dimensional Subsonic-Transonic Compressor Cascade Having Porous-Wall Suction at the Blade Tips. NACA TN 2649, 1952.

12. Winter, K. G.: Comparative Tests of Thick and Thin Turning Vanes in the 4 ft. X 3 ft. Wind Tunnel. AERO. 2217, British R.A.E., Aug. 1947.

13. Thurston, Sidney, and Brunk, Ralph E.: Performance of a Cascade in an Annular Vortex-Generating Tunnel over Range of Reynolds Numbers. NACA RM E51G30, 1951.

14. Stanitz, John D., and Sheldrake, Leonard J.: Application of a Channel Design Method to High-Solidity Cascades and Tests of an Impulse Cascade with 90° of Turning. NACA Rep. 1116, 1953. (Supersedes NACA TN 2652.)

15. Bowen, John T., Sabersky, Rolf H., and Rannie, W. Duncan: Theoretical and Experimental Investigations of Axial-Flow Compressors, pt. 2. Mech. Eng. Lab., C.I.T., July 1949. (Navy Contract N6-ORI-102, Task Order IV.)

16. Preston, J. H., Sweeting, N. E., and Cox, D. K.: The Experimental Determination of the Boundary Layer and Wake Characteristics of a Piercy 12/40 Aerofoil, with Particular Reference to the Trailing Edge Region. R. & M. No. 2013, British A.R.C., Feb. 26, 1945.

17. Cambridge University Aeronautics Laboratory: Measurement of Profile Drag by the Pitot-Traverse Method. R. & M. No. 1688, British A.R.C., Jan. 1936.

18. Wilson, Robert E.: Turbulent Boundary-Layer Characteristics at Supersonic Speeds - Theory and Experiment. Jour. Aero Sci., vol. 17, no. 9, Sept. 1950, pp. 585-594.

TABLE I. - IDENTIFICATION DATA FOR CASCADE AIRFOILS

Number	Airfoil section	Incidence angle, i, deg	Angle of attack, α, deg	Solidity	Chord length, in.	Air inlet angle, deg	Air turning angle, deg	Maximum thickness to chord ratio	Type of cascade tunnel	Inlet Mach number	Blade-chord Reynolds number	Location of measuring plane, x/c	Orientation of measuring plane, perpendicular to -	Instrument used	Reference	Symbol designation
1	65-(12)10 Compressor		16.6	1	3.0	45.0	21.7	0.10	Two-dimensional compressor	0.21	3.6×10^5	0.544	Axial	Multi-tube rake	11	○
2	Thick turning vanes	0		4.0	28.2	47.4	94.8	.066	Two-dimensional impulse	.12	19.0	.460	Wake	Multi-tube rake	12	□
3	Thin turning vanes	0		4.0	28.2	47.4	98.4	.003	Two-dimensional impulse	.12	19.0	.460	Wake	Multi-tube rake	12	◇
4	65-(12)10 Compressor		15	1.038	1.5	45.0	16.3	.10	Annular[a]	.24	1.5	.580	Wake	Multi-tube rake	13	△
5	65-(12)10 Compressor		25	1.038	1.5	45.0	27.0	.10	Annular	.24	1.93	.526	Wake	Multi-tube rake	13	▽
6	Turning vanes	-1.3		1.63	5.5	48.0	90.5	.18	Two-dimensional impulse	.30	9.0	.389	Axial	Probe traverse	14	◿
7	Circular-arc compressor	-3.6		.92	2.8	37.1	15.4	.10	Annular	<.10	0.9	.021, .105, .450	Axial	Probe traverse	15	◸
8	Circular-arc compressor	-8.5		.92	2.8	37.1	13.1	.10	Annular	<.10	0.95	.021	Axial	Probe traverse	15	▷
9	Circular-arc compressor	.4		.92	2.8	37.1	18.7	.10	Annular	<.10	0.8	.450	Axial	Probe traverse	15	◁
10	Circular-arc compressor	-3.5		.92	2.8	37.1	15.5	.10	Annular	<.10	0.9	.450	Axial	Probe traverse	15	○
11	Turbine blade	10.0		1.25	3.09	22.5	60.0	---	Two-dimensional accelerating	.4	8.5	.126, .252, .504, .948	Axial	Probe traverse	4	◇

[a]All data in annular tunnels are at blade mean radius.

TABLE II. - IDENTIFICATION DATA FOR ISOLATED AIRFOILS

Number	Airfoil section	Angle of attack, deg	Chord length, in.	Maximum thickness to chord ratio	Test facility	Blade-chord Reynolds number	Location of measuring plane, x/c	Type of instrument used	Reference	Symbol designation
12	Joukowski	0	20	0.12	4' × 2' Wind tunnel	4.2×10^5	0,.005,.025, .10,.25, .5,.75	Probe traverse	8	▽
13	Joukowski	6	20	.12	4' × 2' Wind tunnel	4.2	0,.005,.025, .10,.25,.50	Probe traverse	8	○
14	Piercy 12/40	0	20	.12	4' × 2' Wind tunnel	4.2	0,.005,.025, .10,.25,.50	Probe traverse	16	▽
15	Piercy 12/40	6	20	.12	4' × 2' Wind tunnel	4.2	0,.005,.025, .10,.25,.40	Probe traverse	16	△
16	Wing section	-	--	.20	Wind tunnel	---	.042,.25, .659,.980	Probe traverse	17	⌂
17	Aircraft wing	-	60	.10	Flight	50	.005,.050, .103,.148	Probe traverse	17	◇
18	NACA 0009	0	72	.09	Full-scale wind tunnel	50	.05,.10,.15,.30, .60,1.0,2.0	Multi-tube rake	9	□
19	NACA 0012	0	72	.12	Full-scale wind tunnel	50	.05,.10,.15,.30, .60,1.0,2.0	Multi-tube rake	9	◇
20	NACA 0018	0	72	.18	Full-scale wind tunnel	50	.05,.10,.15,.30, .60,1.0,2.0	Multi-tube rake	9	◇
21	NACA 0012	for C_L = 0.78	72	.12	Full-scale wind tunnel	50	.05,.10,.15,.30, 1.0,2.0	Multi-tube rake	9	◇

TABLE III. - EQUATIONS FOR $\frac{V}{V_0}$, $\frac{\Delta F_M}{\Delta F_A}$, and K FOR ANALYTICAL WAKE VELOCITY PROFILES OF FIGURE 16

Wake profile	Velocity ratio, $\frac{V}{V_0}$	Averaging ratio, $\Delta F_M/\Delta F_A$	Pseudoenergy factor, K
Linear	$\frac{V_{min}}{V_0} + \left(1 - \frac{V_{min}}{V_0}\right) Y$	$\frac{3}{4} \frac{1 + 2\left(\frac{V_{min}}{V_0}\right) + \left(\frac{V_{min}}{V_0}\right)^2}{\left[1 - \frac{1}{2}\left(\frac{\delta}{s_n}\right)\left(1 - \frac{V_{min}}{V_0}\right)\right]\left(2 + \frac{V_{min}}{V_0}\right)}$	$\frac{H^2 - 2H + 9}{8H}$
Half-sine wave	$\frac{1}{2}\left[\left(1 + \frac{V_{min}}{V_0}\right) - \left(1 - \frac{V_{min}}{V_0}\right)\cos(\pi Y)\right]$	$\frac{1}{2} \frac{3 + 8\left(\frac{V_{min}}{V_0}\right) + 5\left(\frac{V_{min}}{V_0}\right)^2}{\left[1 - \frac{1}{2}\left(\frac{\delta}{s_n}\right)\left(1 - \frac{V_{min}}{V_0}\right)\right]\left[5 + 3\left(\frac{V_{min}}{V_0}\right)\right]}$	$\frac{H^2 - 2H + 10}{9H}$
Quarter-sine wave	$\frac{V_{min}}{V_0} + \left(1 - \frac{V_{min}}{V_0}\right) \sin\left(\frac{\pi}{2} Y\right)$	$\frac{\frac{2}{3\pi} - \left(\frac{1}{2} - \frac{8}{3\pi}\right)\left(\frac{V_{min}}{V_0}\right) + \left(\frac{3}{2} - \frac{22}{3\pi}\right)\left(\frac{V_{min}}{V_0}\right)^2}{\left[1 - \left(\frac{\delta}{s_n}\right)\left(1 - \frac{2}{\pi}\right)\left(1 - \frac{V_{min}}{V_0}\right)\right]\left[\frac{1}{2} + \left(\frac{3}{2} - \frac{4}{\pi}\right)\left(\frac{V_{min}}{V_0}\right)\right]}$	$\frac{1}{H}\left[(f - 1)H^2 - 2(f - 1)H + f\right]$ $f = \frac{2}{3} \frac{(15\pi - 44)(\pi - 2)}{(3\pi - 8)^2}$
Error curve	$1 - \left(1 - \frac{V_{min}}{V_0}\right) e^{-gY^2}$ $g = \ln\left[100\left(1 - \frac{V_{min}}{V_0}\right)\right]$	$\frac{\left(1 - \frac{3}{2\sqrt{2}} + \frac{1}{2\sqrt{3}}\right) + \left(\frac{3}{2\sqrt{3}} - \frac{1}{\sqrt{3}}\right)\left(\frac{V_{min}}{V_0}\right) + \frac{1}{2\sqrt{3}}\left(\frac{V_{min}}{V_0}\right)^2}{1 - \left(\frac{\delta}{s_n}\right)\frac{\sqrt{\pi}}{2\sqrt{g}}\left(1 - \frac{V_{min}}{V_0}\right)\left(1 - \frac{1}{2\sqrt{2}}\right) + \frac{1}{2\sqrt{2}}\left(\frac{V_{min}}{V_0}\right)}$ $g = \ln\left[100\left(1 - \frac{V_{min}}{V_0}\right)\right]$	$\frac{1}{H}\left[(f - 1)H^2 - 2(f - 1)H + f\right]$ $f = \frac{2}{\sqrt{3}}$
Power	Y^m		$\frac{H + 1}{3H - 1}$

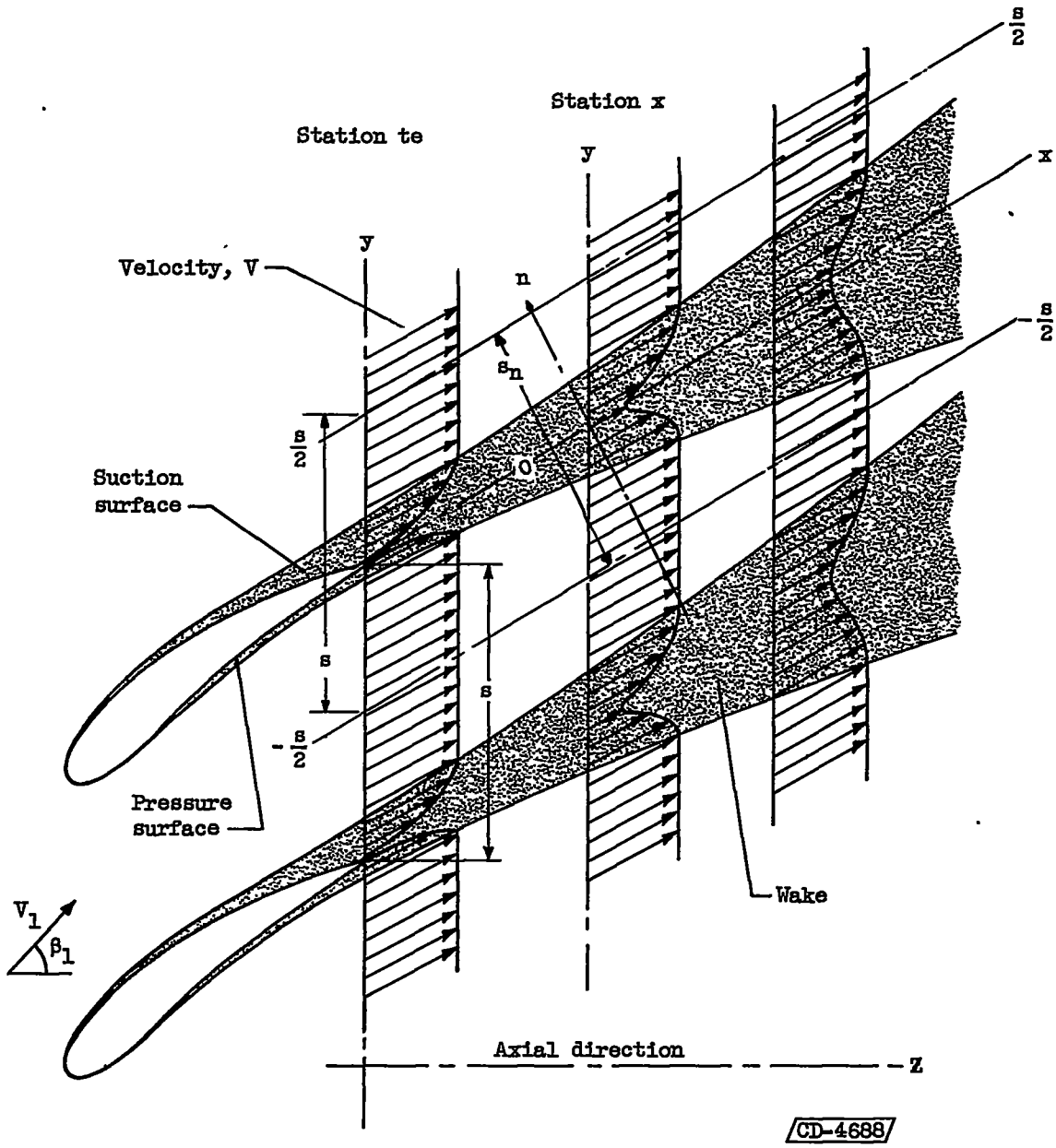

Figure 1. - Schematic representation of wake development in flow about cascade blade sections.

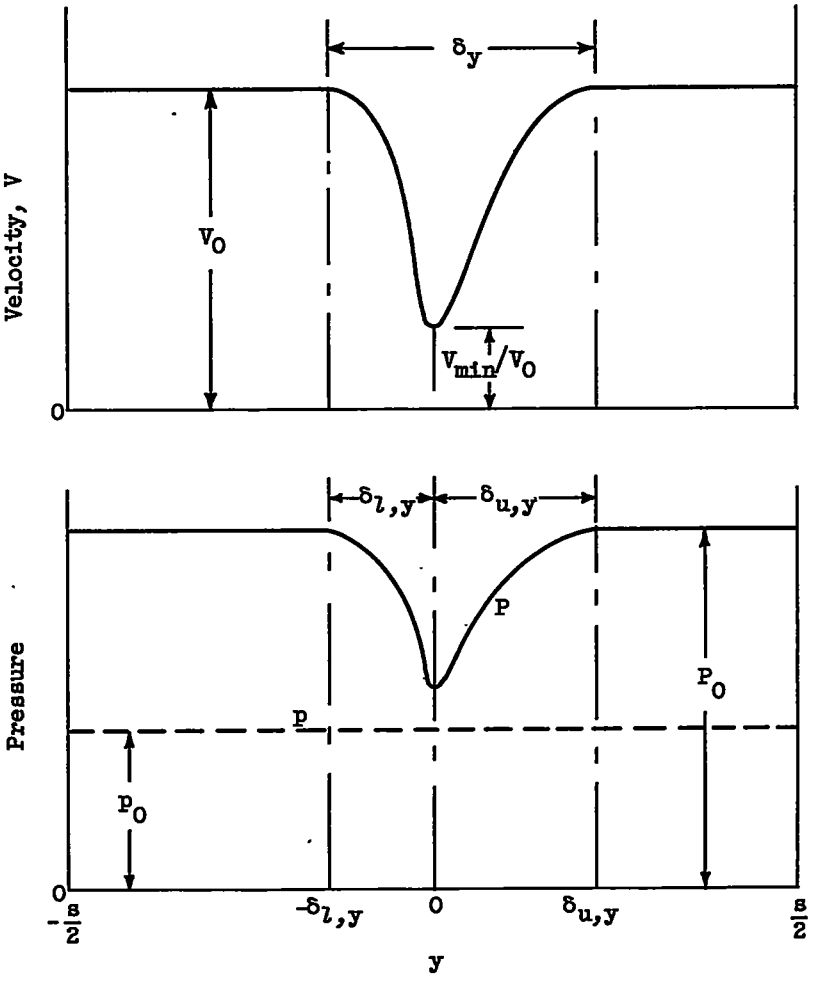

Displacement thickness:
$$\delta_y^* = \delta_{u,y}^* + \delta_{l,y}^* = \int_{-\delta_{l,y}}^{\delta_{u,y}} \left(1 - \frac{V}{V_0}\right) dy; \quad \delta^* = \delta_u^* + \delta_l^* = \delta_y^* \cos \beta$$

Momentum thickness:
$$\theta_y = \theta_{u,y} + \theta_{l,y} = \int_{-\delta_{l,y}}^{\delta_{u,y}} \left(1 - \frac{V}{V_0}\right)\frac{V}{V_0} dy; \quad \theta = \theta_u + \theta_l = \theta_y \cos \beta$$

Pseudoenergy thickness:
$$k_y = k_{u,y} + k_{l,y} = \int_{-\delta_{l,y}}^{\delta_{u,y}} \left(1 - \frac{V}{V_0}\right)\left(\frac{V}{V_0}\right)^2 dy; \quad k = k_u + k_l = k_y \cos \beta$$

$$H = \frac{\delta^*}{\theta} = \frac{\delta_y^*}{\theta_y}, \qquad K = \frac{k}{\theta} = \frac{k_y}{\theta_y}, \qquad \delta = \delta_u + \delta_l = \delta_y \cos \beta$$

Figure 2. - Model variation of velocity and pressure in plane normal to axial direction and definitions of wake properties. (Subscript y refers to wake properties in plane normal to axial direction; no subscript indicates properties in plane normal to outlet flow.)

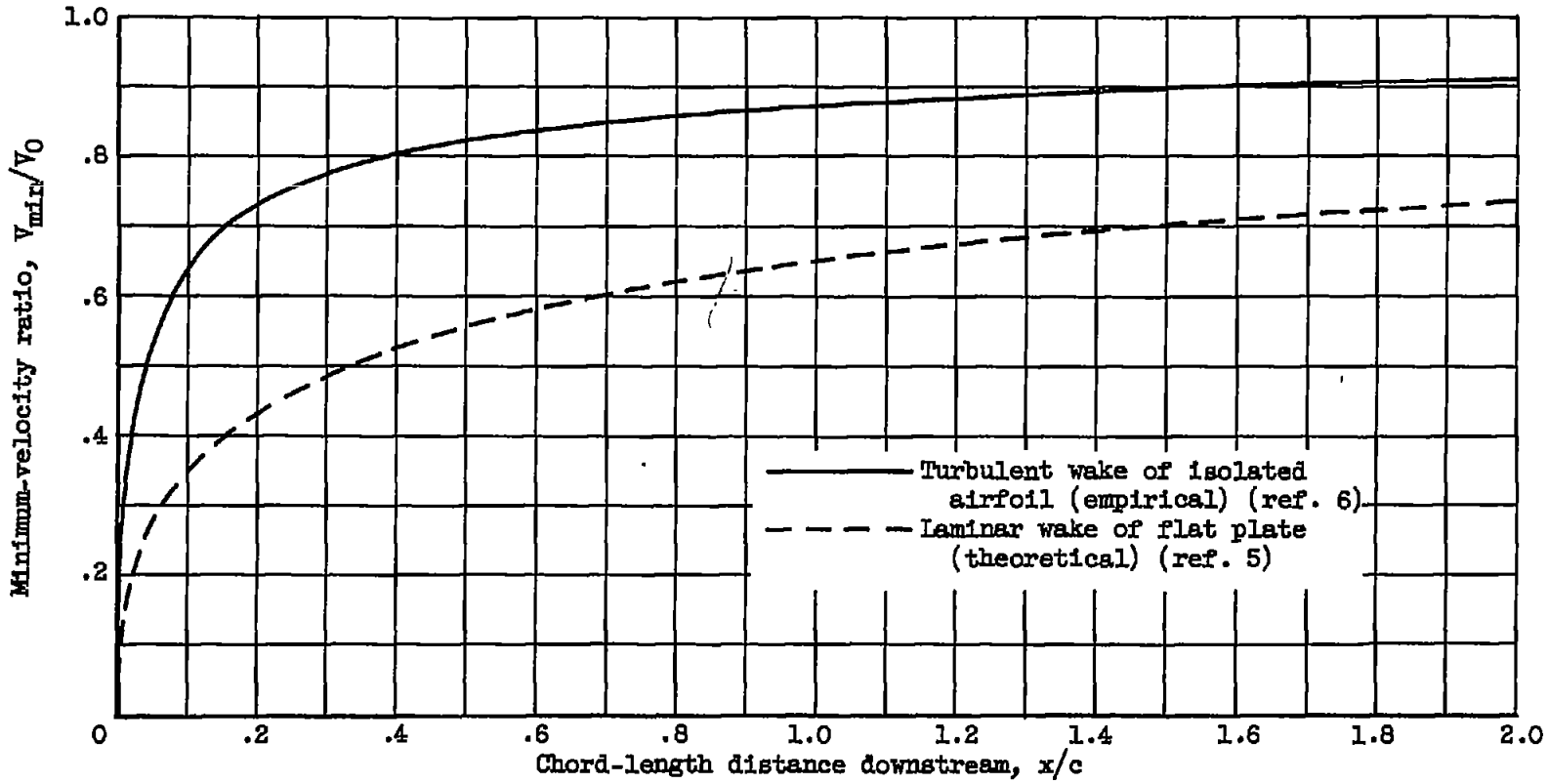

Figure 3. - Recovery of minimum velocity in wake of solid bodies downstream of trailing edge.

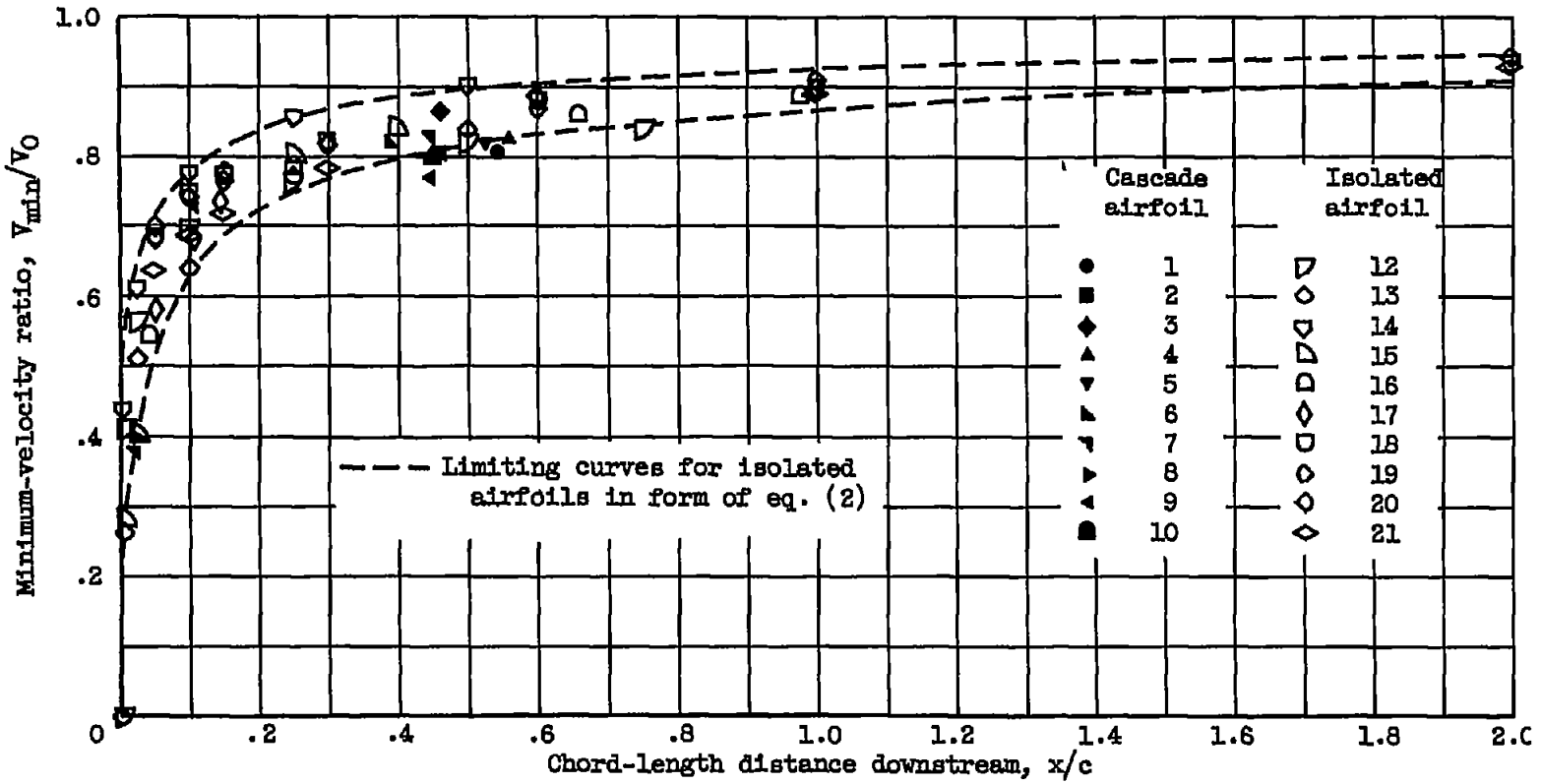

Figure 4. - Experimental downstream variation of recovery of minimum velocity in wake of cascade and isolated airfoils.

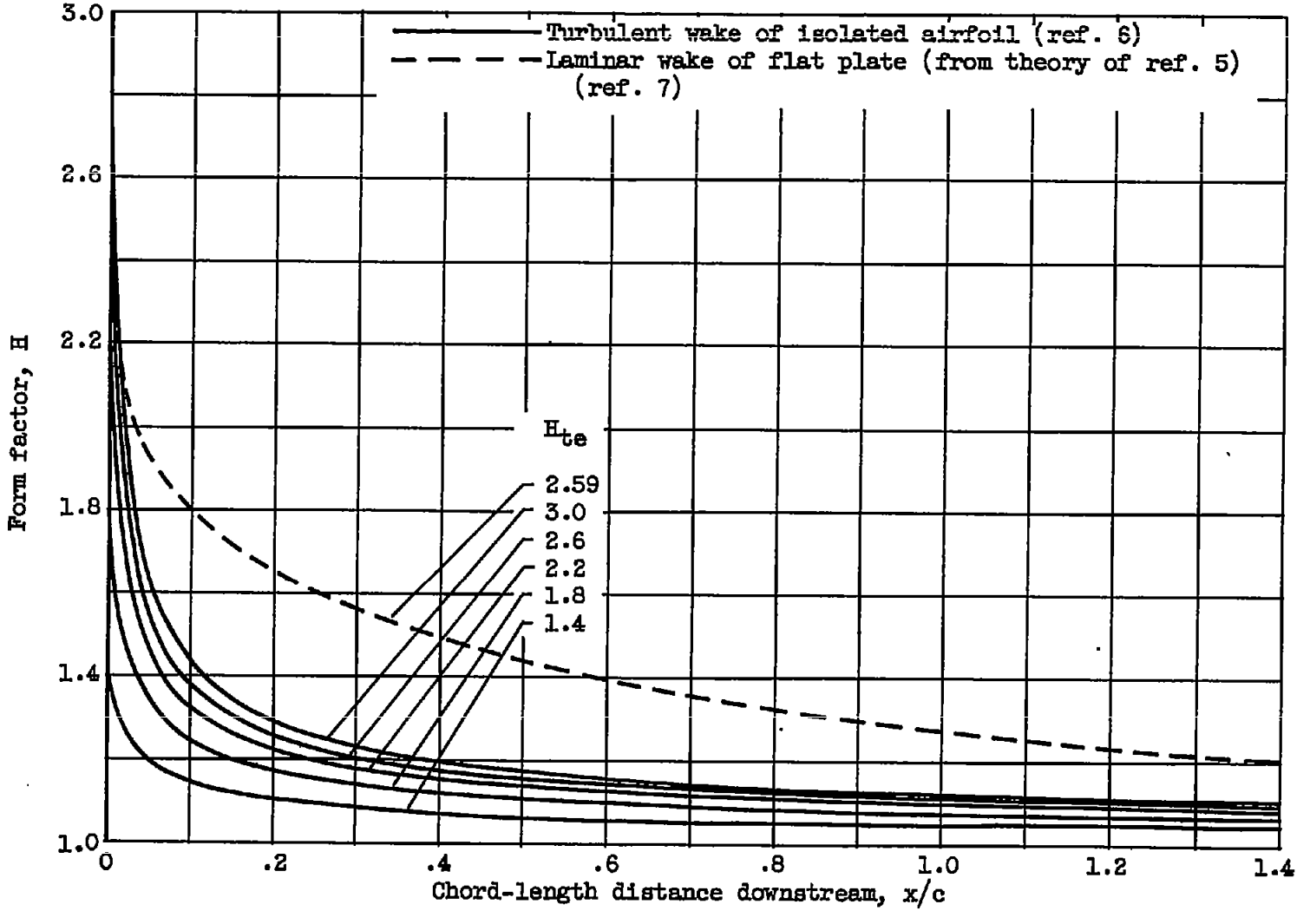

Figure 5. - Theoretical variation of wake form factor with distance downstream of trailing edge of solid bodies.

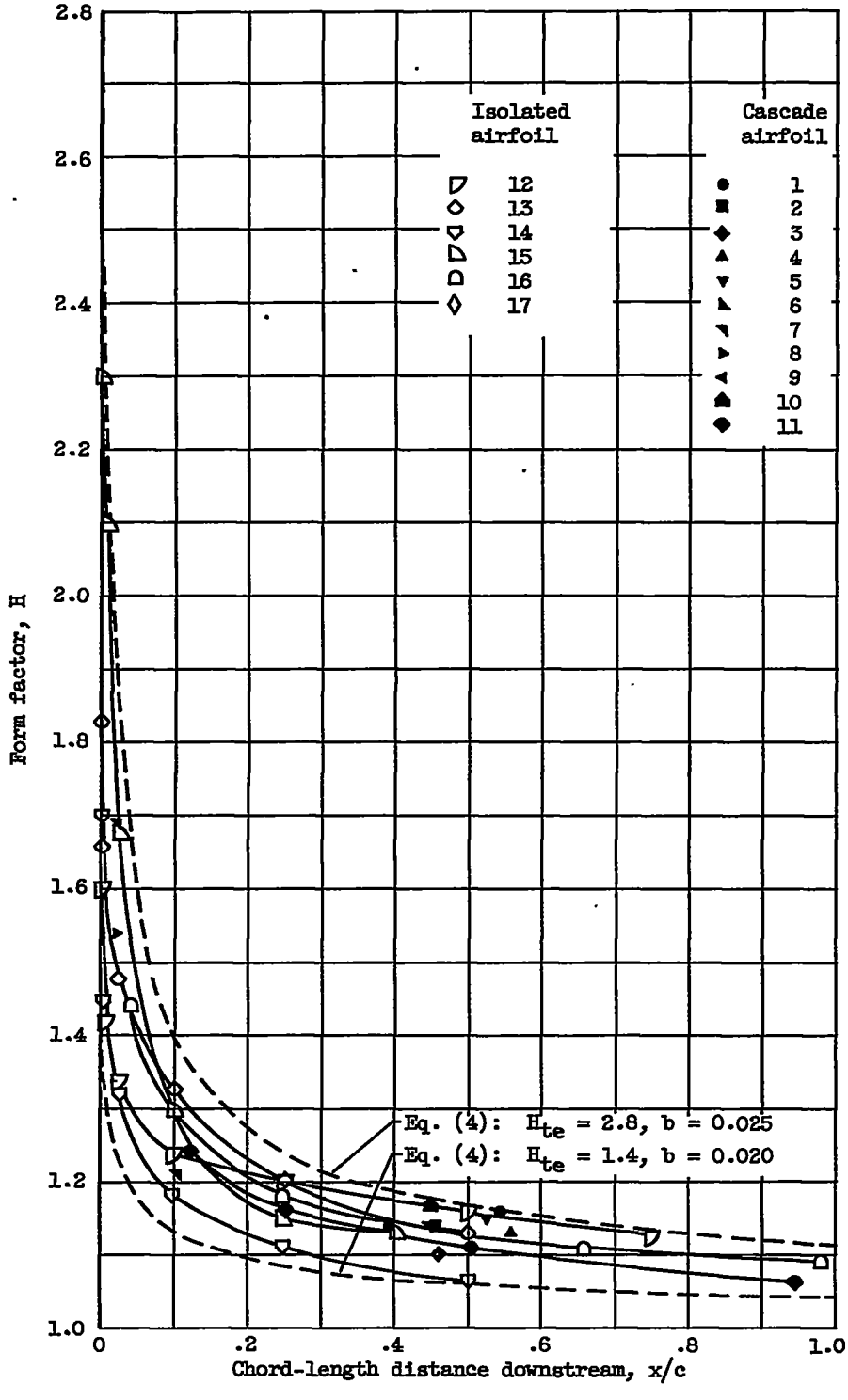

Figure 6. - Experimental downstream variation of wake form factor for cascade and isolated airfoils.

4000

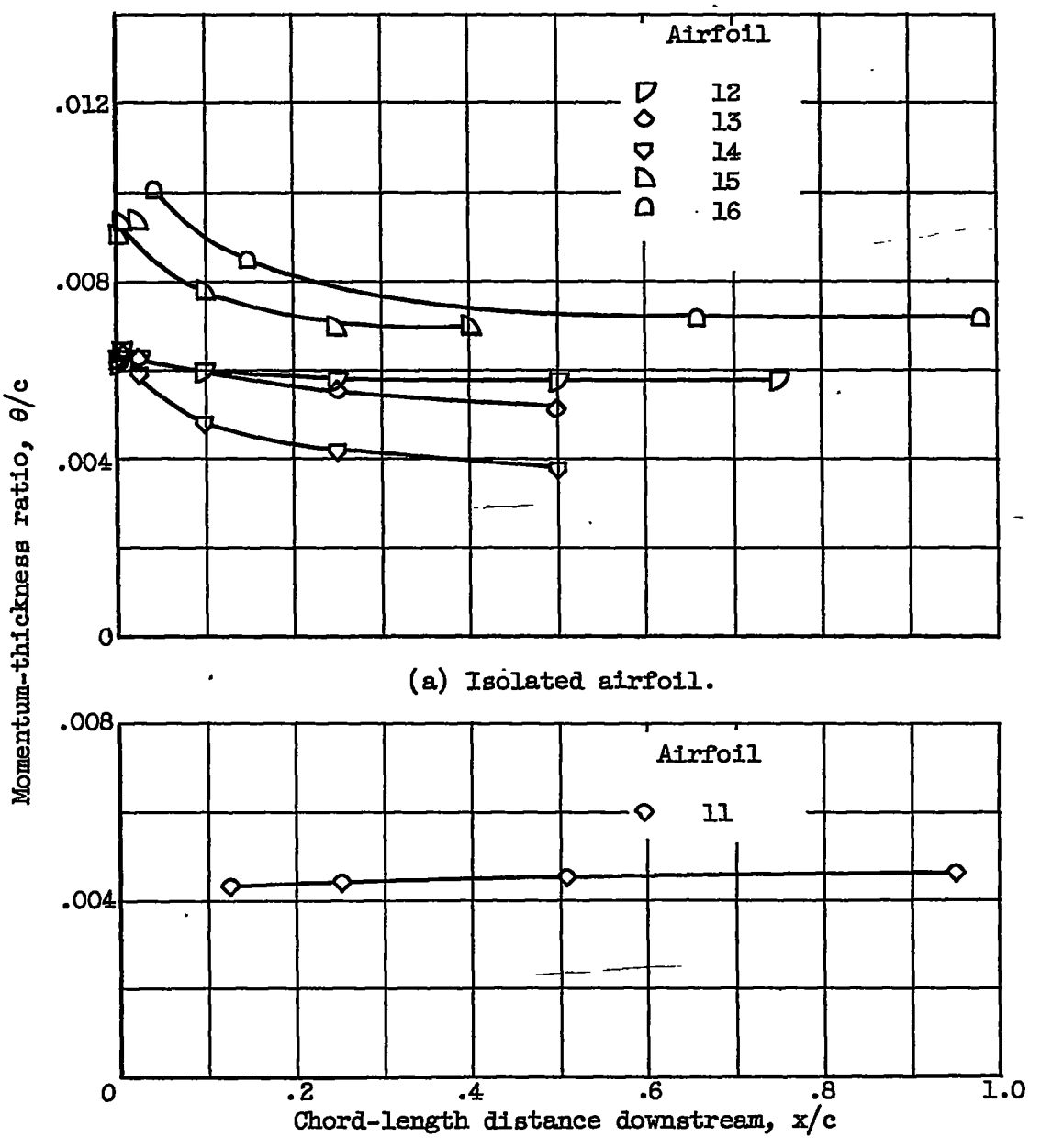

(b) Cascade airfoil.

Figure 7. - Experimental downstream variation of wake momentum thickness for cascade and isolated airfoils.

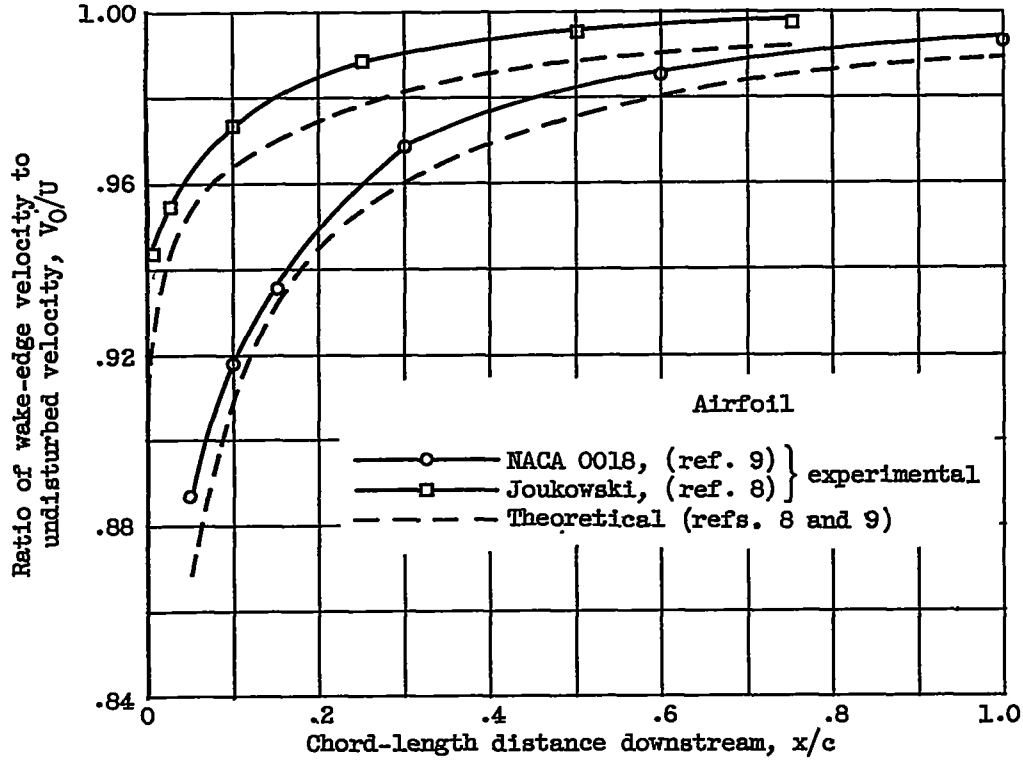

Figure 8. - Typical variation of wake-edge velocity for isolated airfoils.

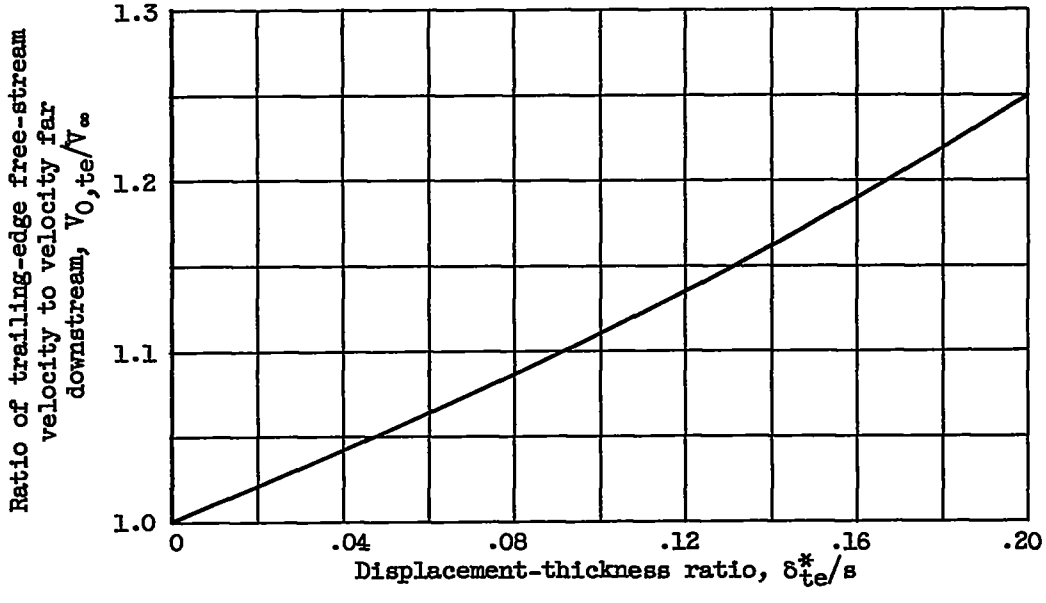

Figure 9. - Theoretical variation of ratio of free-stream velocity at trailing edge to velocity far downstream for cascade airfoil.

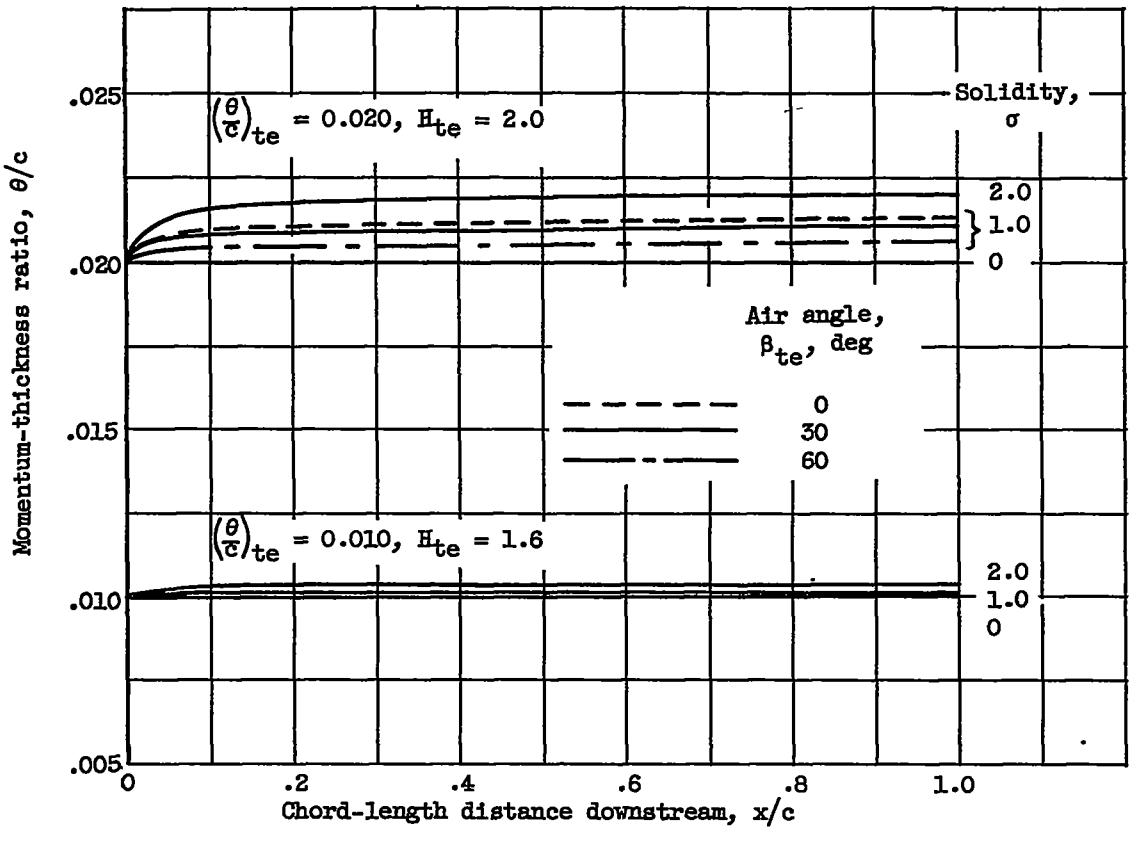

Figure 10. - Theoretical downstream variation of cascade wake momentum thickness due to cascade continuity effect.

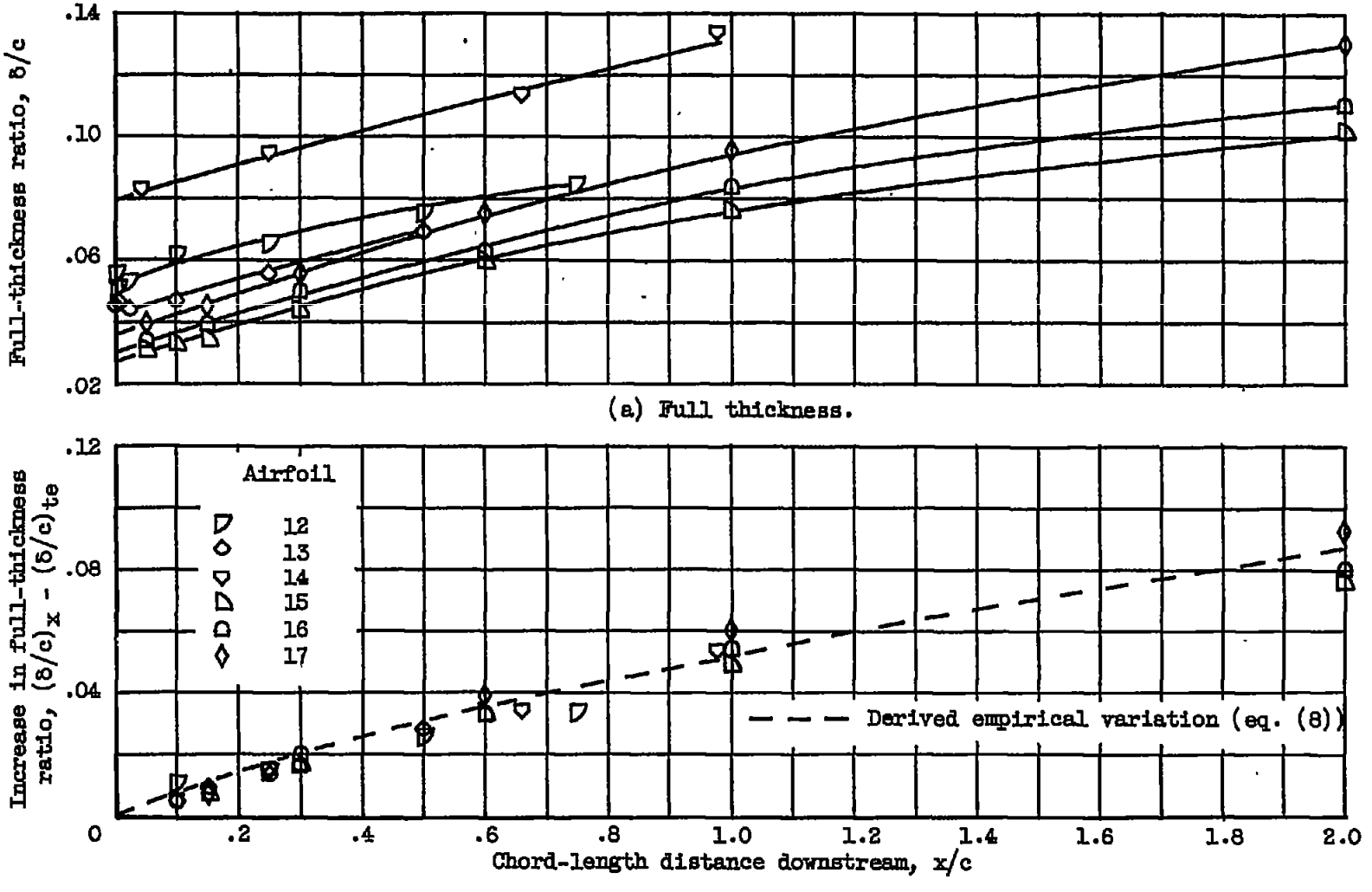

Figure 11. - Experimental downstream variation of wake full thickness for isolated airfoils.

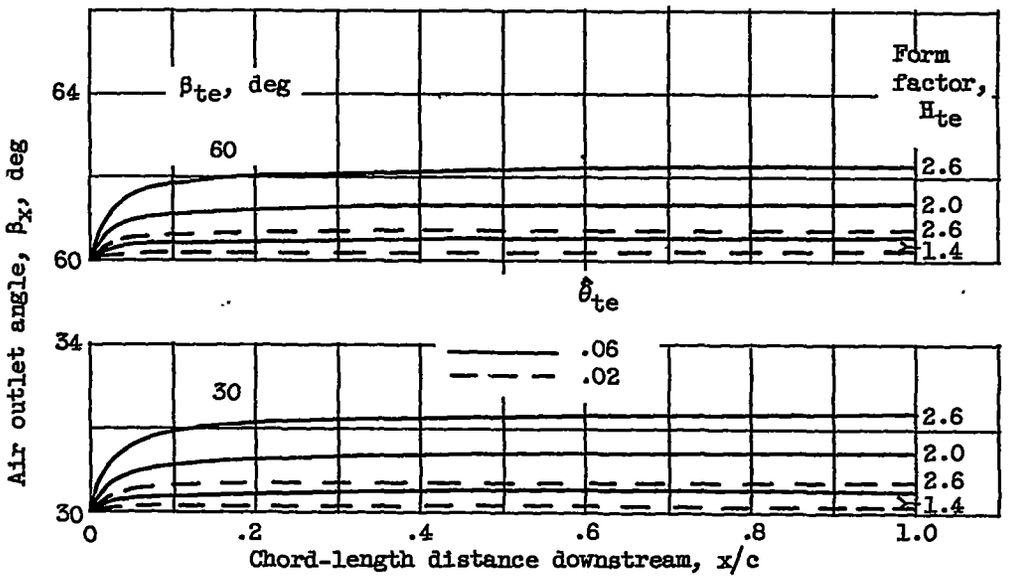

Figure 12. - Theoretical downstream variation of air outlet angle for cascade airfoil.

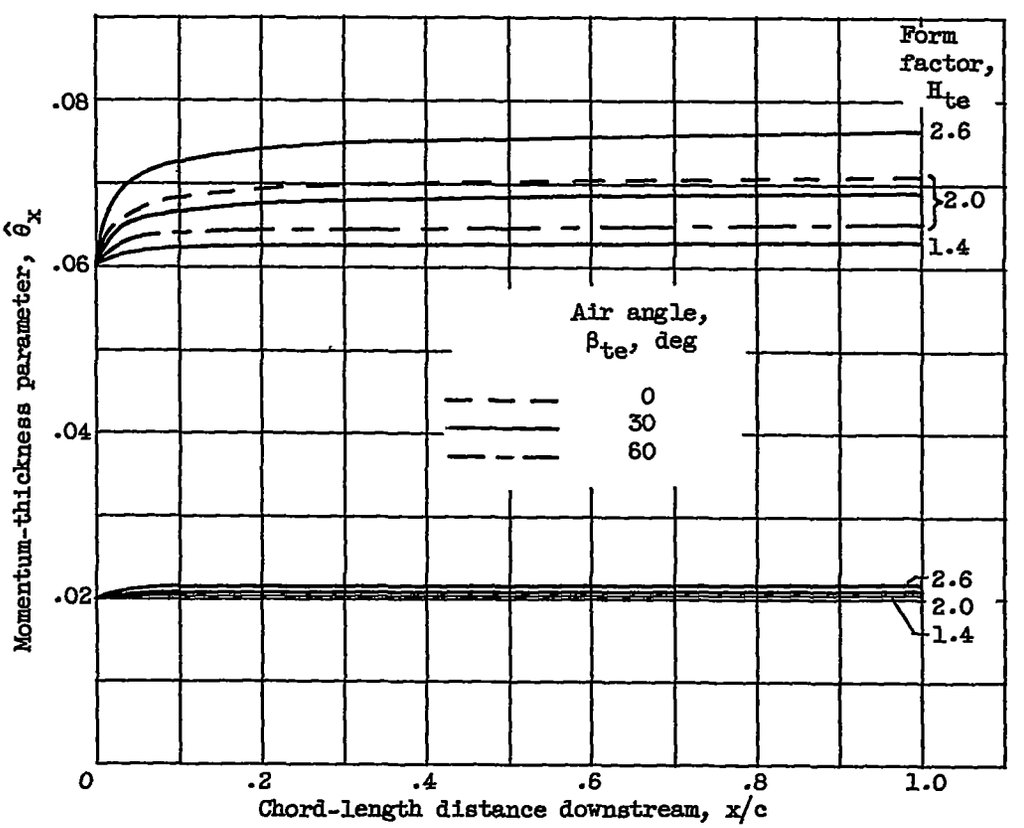

Figure 13. - Theoretical downstream variation of wake momentum-thickness parameter for cascade airfoil.

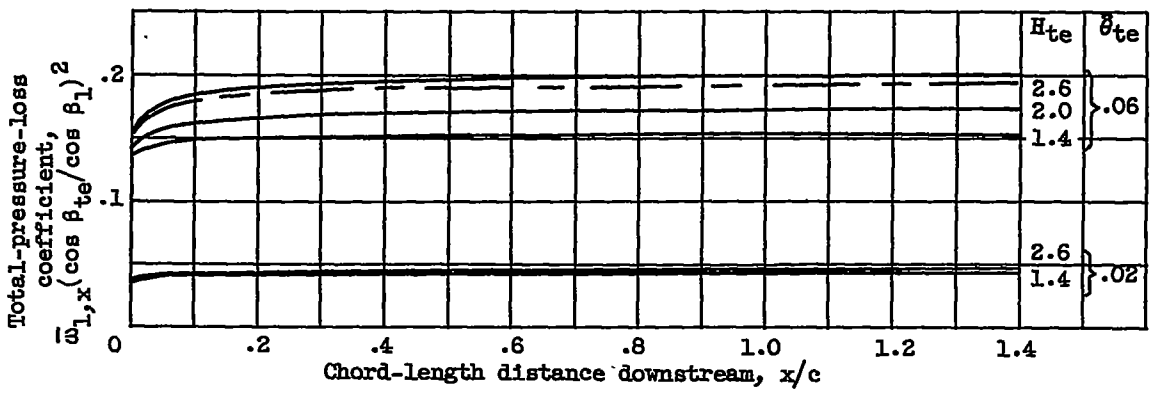

Figure 14. - Theoretical downstream variation of total-pressure-loss coefficient for cascade airfoil.

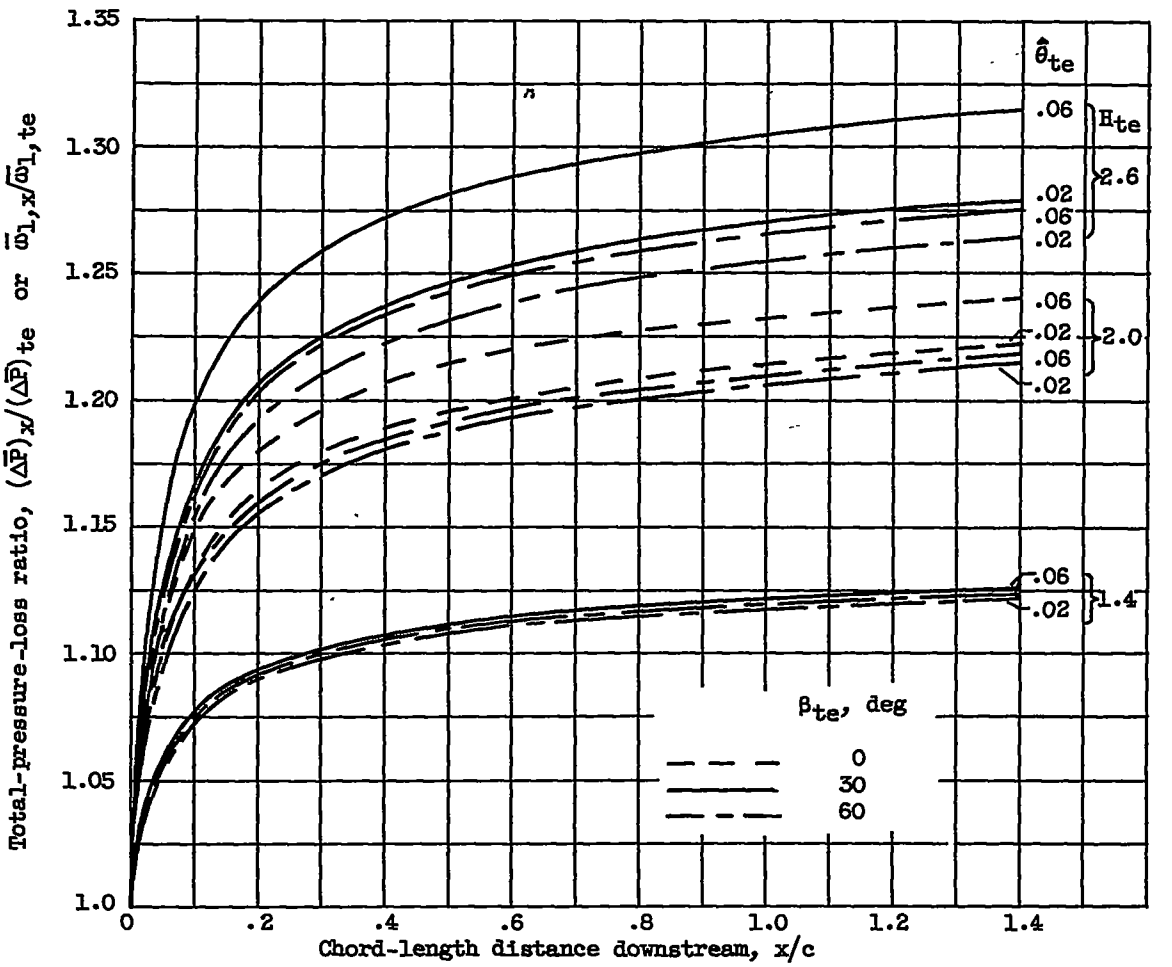

Figure 15. - Theoretical downstream variation of total-pressure-loss ratio for cascade airfoil.

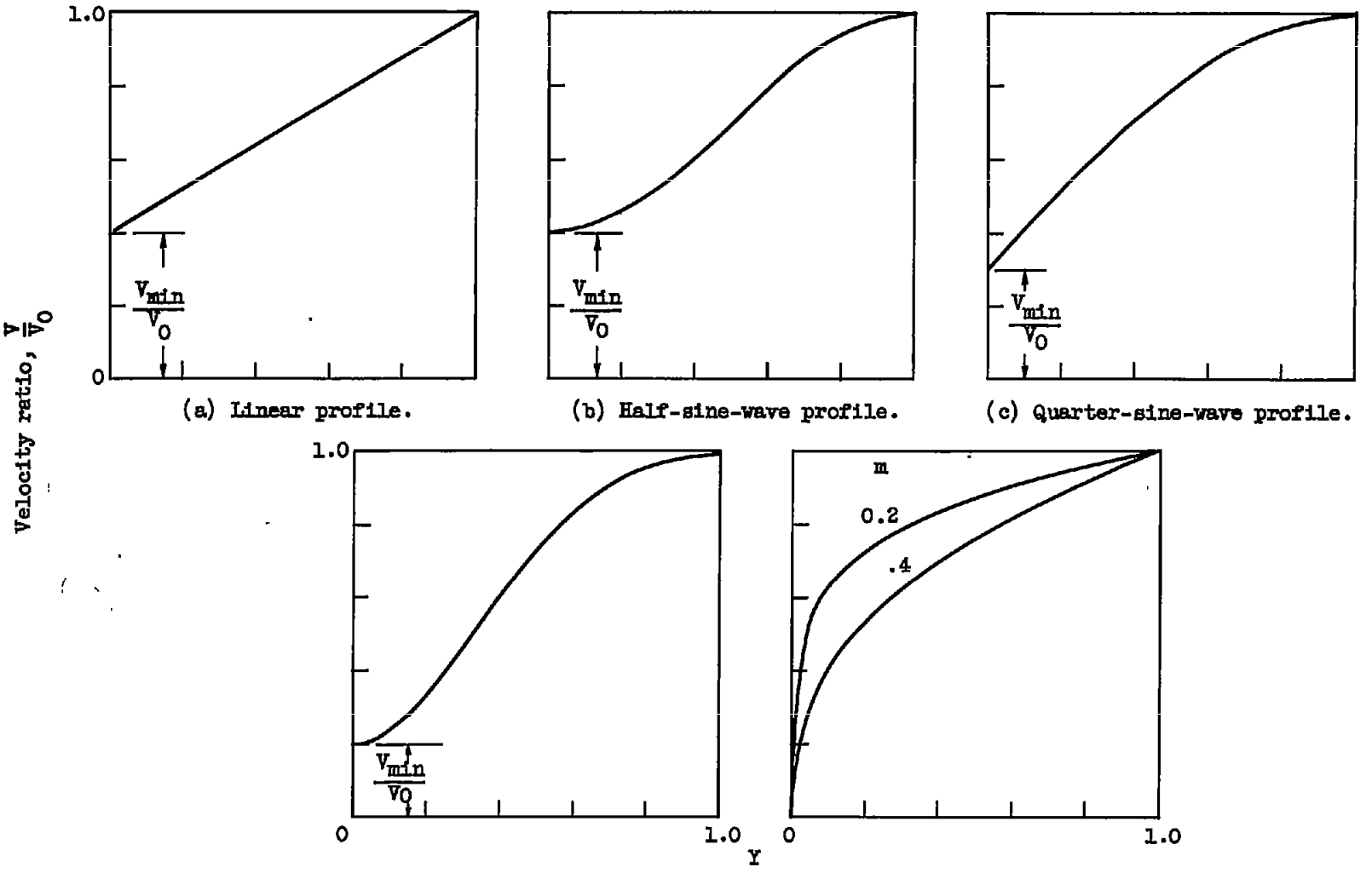

Figure 16. - Analytical velocity profiles in half wake used in analysis of wake properties.

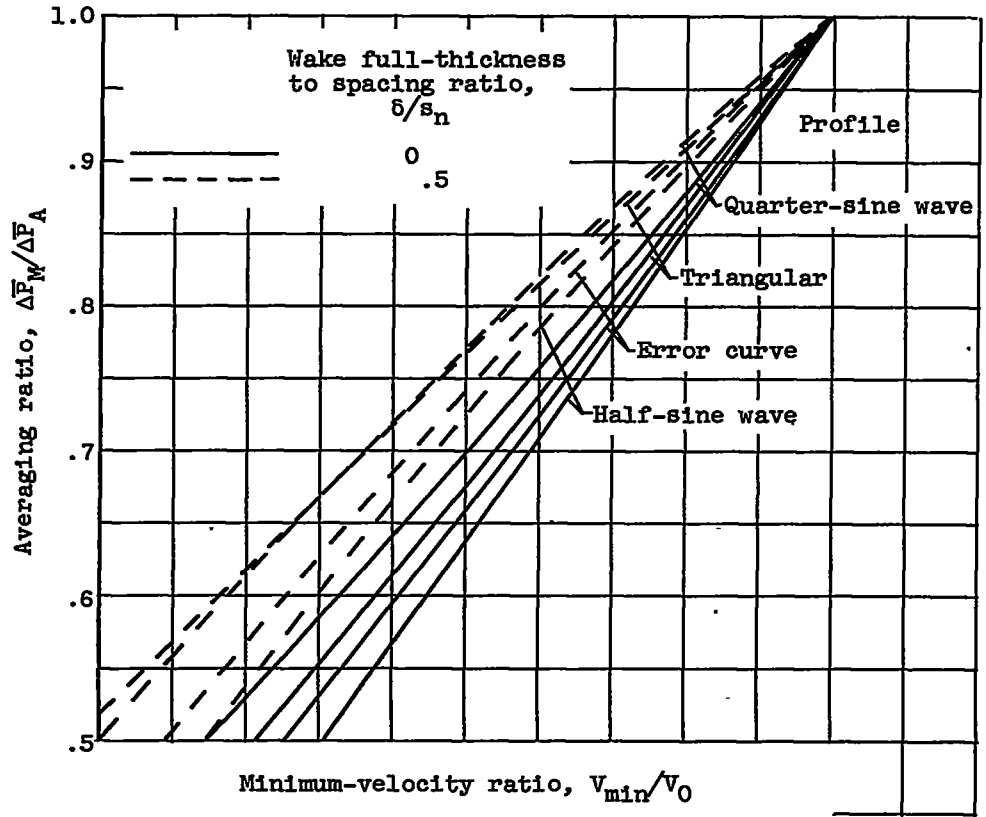

(a) Variation with wake-minimum-velocity ratio.

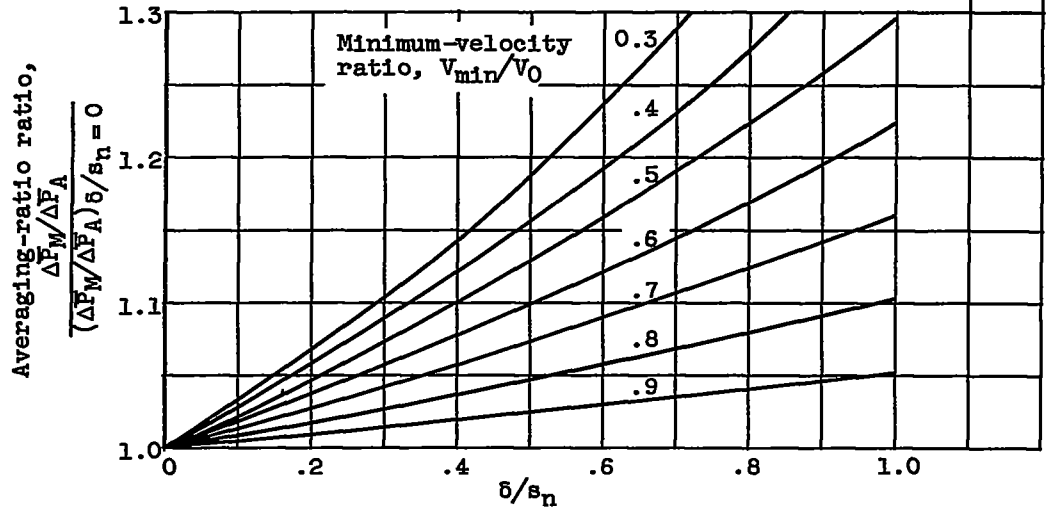

(b) Variation with wake full-thickness to spacing ratio (average of all profiles).

Figure 17. - Theoretical ratio of mass-averaged to area-averaged defect in total pressure for representative analytical wake-velocity profiles.

4000

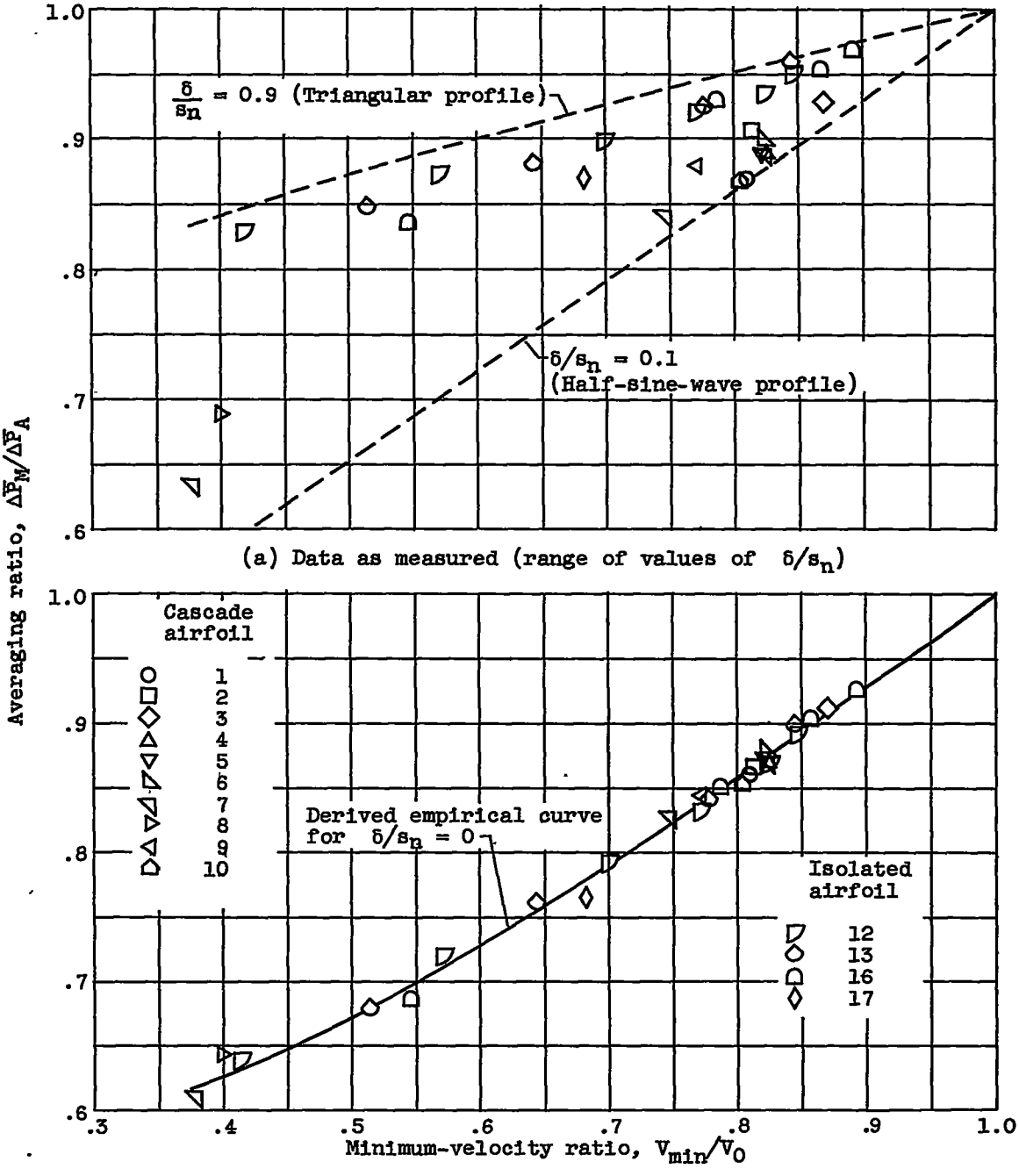

(a) Data as measured (range of values of δ/s_n)

(b) Data corrected to $\delta/s_n = 0$ according to figure 17(b).

Figure 18. - Experimental values of ratio of mass-averaged to area-averaged defect in total pressure in blade wake.

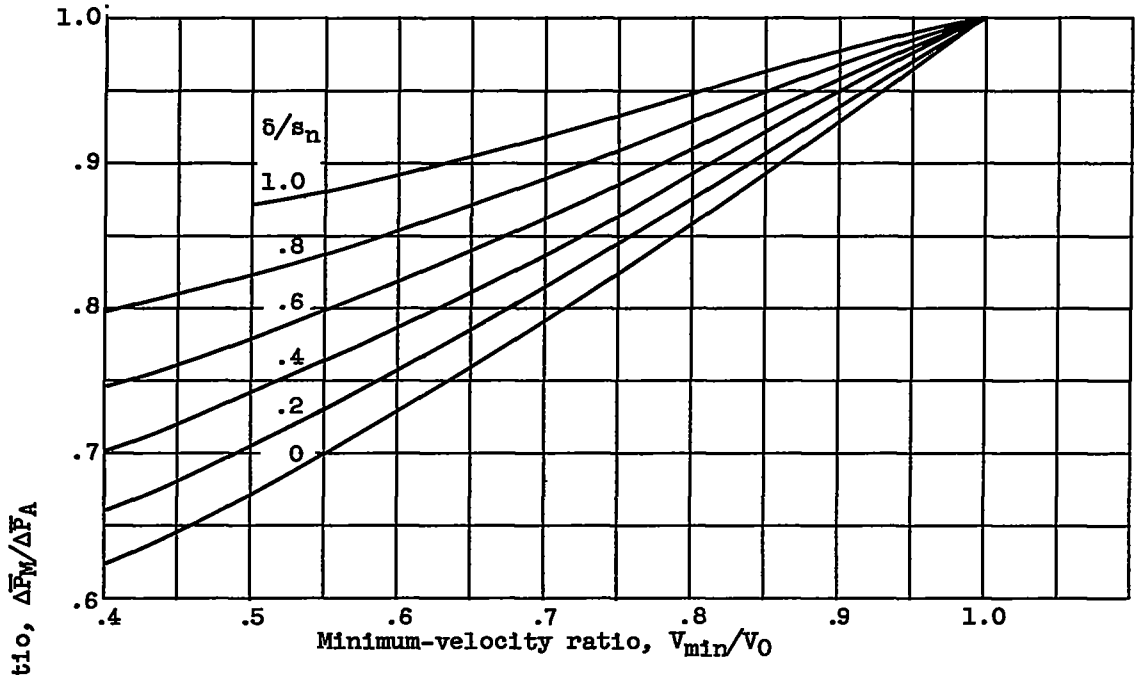

(a) Variation with wake minimum-velocity ratio (from figs. 17(b) and 16(b)).

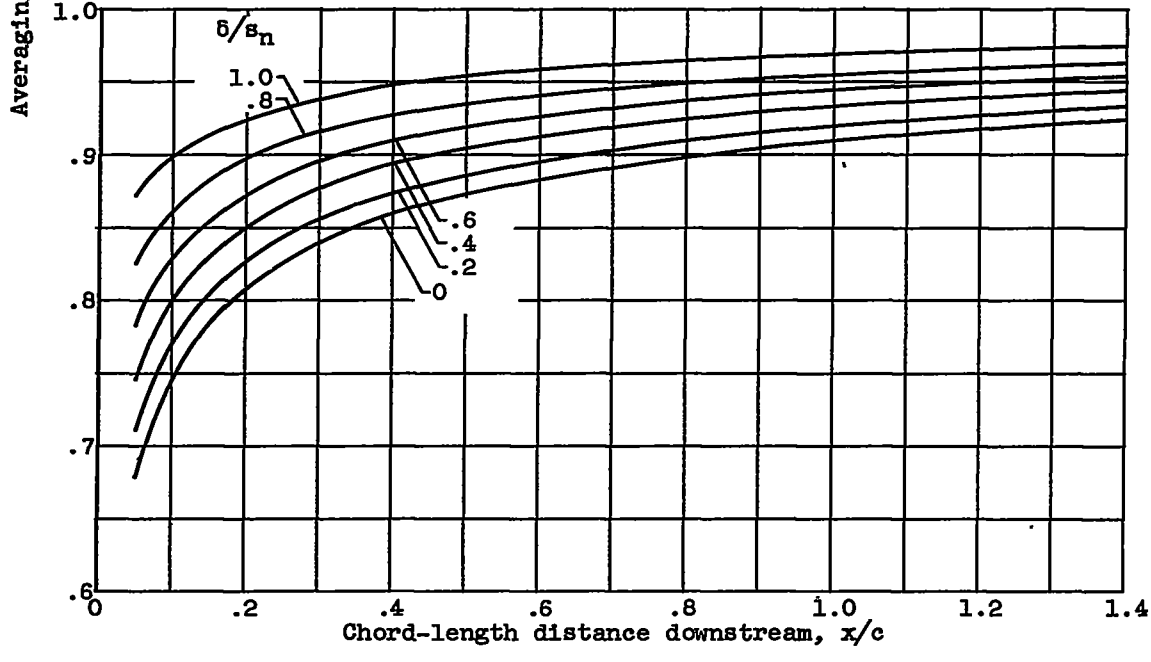

(b) Variation with distance downstream of trailing edge (from (a) and eq. (3)).

Figure 19. - Derived variation of ratio of mass-averaged to area-averaged defect in total pressure in blade wake.

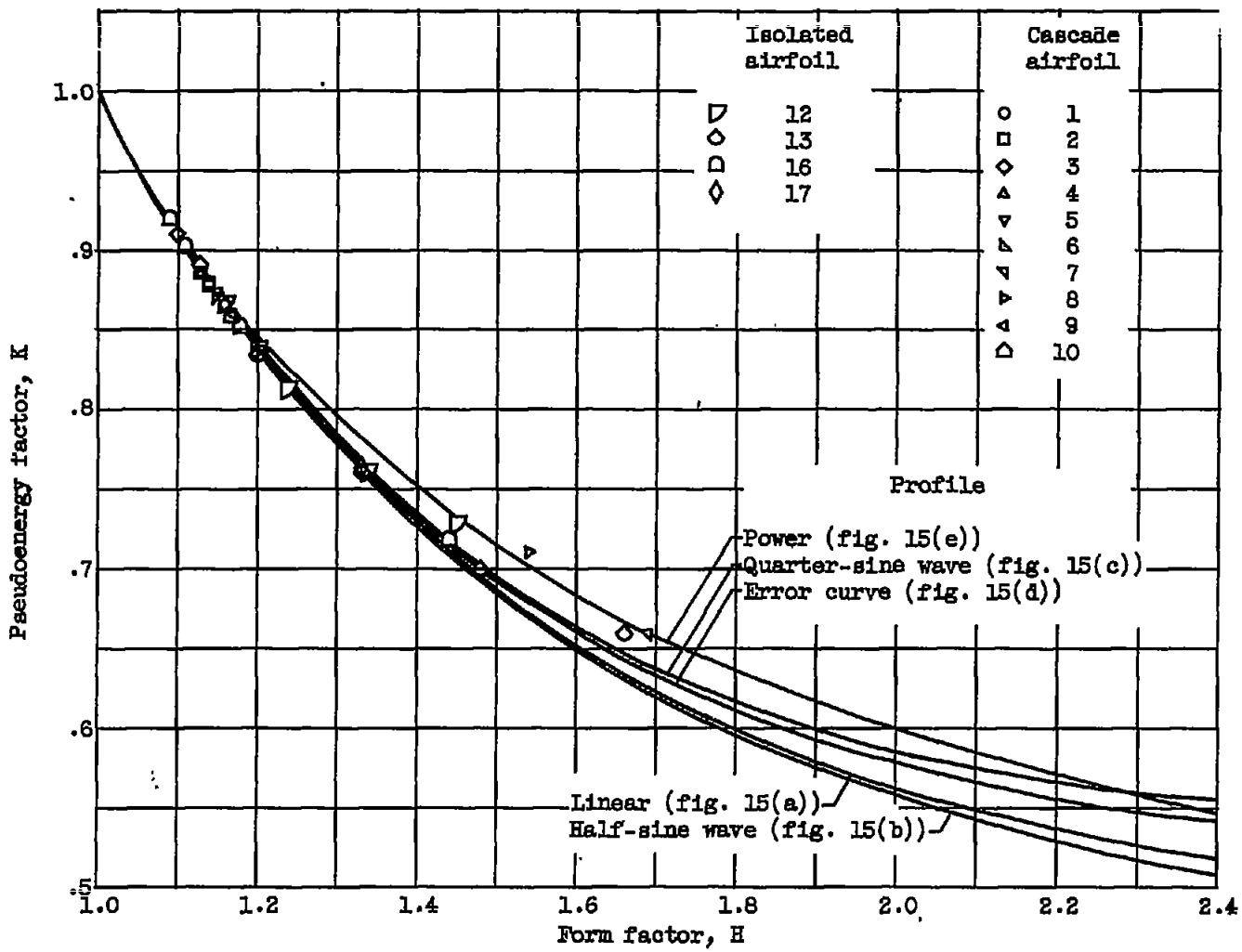

Figure 20. - Experimental variation of wake pseudoenergy factor with wake form factor for isolated and cascade airfoils for minimum velocity in wake greater than zero ($0.02 < x/c$).